

Final LDRD Report on a Novel Interferometric Spectrometer for the Doppler Planet Search

98-ERD-054

David J. Erskine, Jian Ge, Mike Rushford and Bruce Macintosh
Lawrence Livermore National Lab., Livermore, CA 94550

Contact: erskine1@llnl.gov

ABSTRACT

This report describes the results of the LDRD funded project (98-ERD-054) to develop a novel interferometric spectrometer for the Doppler planet search, called an externally dispersed interferometer (EDI). A new kind of spectroscopy has been invented that combines the best features of purely dispersive and purely interferometric techniques. The invention is expected to fill some roles now performed by the Fourier Transform Spectrometer, and other roles now performed by large high resolution grating spectrometers.

In comparison to the FTS, the EDI 1) Is much more efficient in low light level applications where photon noise dominates; 2) Can operate with no moving parts and therefore record single-shot events (e.g., diagnostics of explosions).

In comparison to a high resolution (R=60 k) grating spectrograph, the EDI 1) Is much smaller, lower weight and therefore can be put on airborne or spaceborne platforms where previously not practical; 2) Is theoretically much more robust to a variety of environmentally induced errors, further reducing cost; 3) Can be rapidly built using off the shelf components; 4) Portable; 5) Wider field of view increases photon flux for extended objects, such as stars blurred by the atmosphere; 6) Has a demonstrated velocity precision which already approximately matches the state of the art and is likely to exceed it with further development.

Potential applications include:

1) Doppler velocimetry using 'white' or natural light: a) The search for extrasolar planets; b) Real-time measurement of motion of a stellar photosphere (asteroseismology) which probes the interior of a star; c) Improved and more rapid determination of orbit of asteroids or other sunlit bodies using radial velocity; d) Passive (surreptitious) determination of closing velocity of a target, such as between one Earth orbiting satellite and another, using natural sunlight. Previously, spacebased use of high resolution spectrometers was prohibited due to their large (5-meter) size and great mass.

2) Measurement of lineshape asymmetry to study photosphere dynamics.

3) Mapping of the shape of a spectrum. Astrophysics and remote sensing applications.

4) Metrology: measurement of an absolute distance to 0.025 nanometer precision (1 part in 3×10^8): a) High precision sensors that measure a secondary effect such as acceleration, magnetic field etc. that change the delay, without the fringe-skip errors of monochromatic systems. b) Measurement of angular positions of a star or other target using long baseline interferometer. The EDI measures fringe shifts to a precision of $1/20000^{th}$ of a wave, an order of magnitude better than monochromatic or equal-pathlength systems. The EDI could mean smaller and more accurate spacebased instruments hunting for Earth-like planets.

Due to the limited duration of the project only the Doppler velocimetry applications have been demonstrated in experiments. The other potential applications remain to be developed.

Part I summarizes main results and ideas.

Part II Describes observatory test and data reduction details.

Part I

Summary of Main Results and Ideas

1. Introduction

Currently there are more than several dozen known extra-solar planets orbiting nearby stars. The discovery of these planets has captured the interests of both astronomers and the general public. From a scientific perspective, the diversity of these planetary systems has challenged conventional theories of planet formation, providing insight about processes that may have shaped our own solar system.

Most of the planets have been discovered using precision radial velocity measurements using grating spectrometers (reviewed by Marcy & Butler 1998) with demonstrated long term accuracy approaching 3 m/s (Butler et. al., 1996) for the best instrument. Many other instruments currently being used are in the 10 m/s range. The gravitational pull of the exoplanet on the star moves the star in an elliptical motion over days, months or years. This motion generates a sinusoidally varying Doppler shift in the stars spectrum, having amplitudes from a few to hundreds of m/s. A Jupiter-mass planet orbiting at Jupiter-like distance would generate a 12 m/s amplitude velocity signature. An analogous example of this is the monthly Doppler signature is found in the Earth-moon system (Fig. 1). Coincidentally, the 12 m/s amplitude of the moon pulling the Earth is the same as amplitude as Jupiter pulling the sun, making this solar Doppler measurement a relevant and convenient test for a new velocimeter. This was one of the successful milestones accomplished by this project.

1 m/s scale precision desired

Many of the exoplanets found to date have roughly Jovian mass, but orbital periods of only a few days—very different from the 12 year period of our own Jupiter. Recent models of planetary formation suggest that these planets may have migrated towards the star from larger orbits, sweeping away any terrestrial planets (Lin, Bodenheimer, & Richardson 1996), perhaps affecting the ubiquity of habitable planets. In any case, the search for planets with more solar system-like characteristics: lower mass and larger orbital radii, remains intrinsically interesting and these

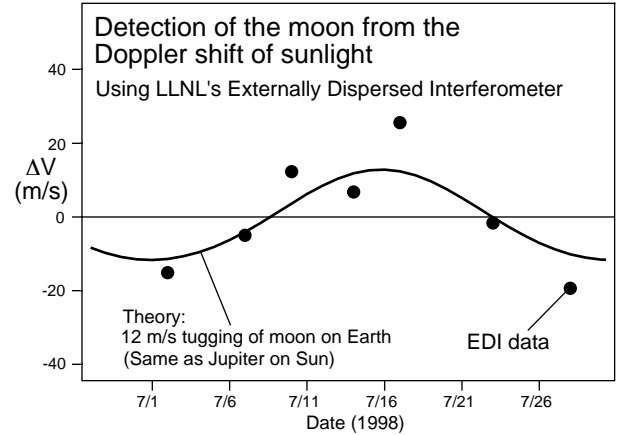


Fig. 1.— An important project milestone was successfully achieved by detecting the 12 m/s Doppler shift in sunlight caused by the tugging of the moon on the Earth. Sunlight was measured using the new instrument (EDI) over a month. The effects of the Earths orbit and daily rotation have been subtracted, leaving the 12 m/s amplitude wobble caused by the moons gravitational pull. This is the same size effect as a Jupiter-like planet pulling a star, demonstrating the prototype already has enough short and long term velocity precision to detect most exo-planets if adequate light intensity is presented to the instrument. The 8 m/s errors seen here are believed not due to the EDI, but due to pointing errors of the heliostat against the 4000 m/s velocity gradient of the solar disk. Such errors would not be involved in stellar observations, where the stellar disk is unresolvable.

will have smaller velocity signatures than the 10–100 m/s usually found now. Hence improving the velocity precision of current instruments from 3–15 m/s to ~ 1 m/s is desired. Also the search for long orbit (multi-year) planets will inevitably involve observations over less than a full orbit. These would also benefit from increased velocity precision, particularly if one planets signature needs to be separated from other, larger signatures of companion bodies.

High light transmission and robustness to environmental insults are other important desired qualities. We introduce a new spectroscopy teaching called the external dispersed interferometer (EDI) that theoretically has all these qualities.

1.1. Current method: purely dispersive spectroscopy

The current method for measuring Doppler shifts of starlight is to disperse the starlight spectrum into many separate intensity channels detected by a CCD detector. The dispersion is accomplished by a large diffraction grating imaging light over large optical

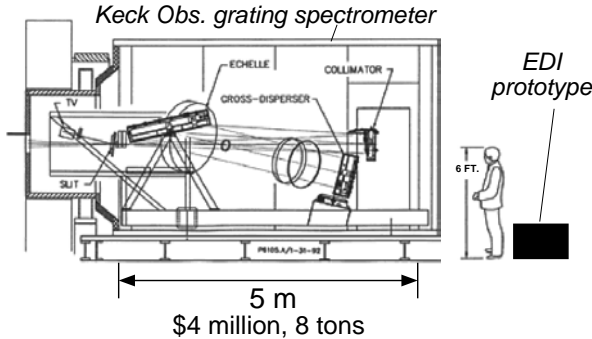


Fig. 2.— Comparison in size between state of the art conventional high resolution spectrometer used for Doppler velocimetry and the EDI prototype. In the conventional method large optics separated by large distances must be rigidly mounted to tight dimensional tolerances. This requires massive mechanical supports, driving up costs and preventing airborne or spaceborne operation. The EDI can be an orders of magnitude smaller in volume, mass and cost because the optical tolerances of its disperser component are much looser. The interferometer component of the EDI must have high optical quality, but since this is only a few centimeters in size this is easy to achieve using off-the-shelf components. The reduction in net instrument volume especially lowers the cost for infrared spectroscopy, where the entire instrument must be cooled.

pathlengths. This requires large, massive and expensive optics having very sturdy mechanical mounts and housed in an environmentally controlled room. The spectrographs can be several meters long (kitchen-sized). One of the most precise such instruments is the grating spectrometer at Keck Observatory, whose plan is shown in Fig. 2 (5 m length). The Hamilton spectrograph at Lick Observatory is similarly sized (7 m length). (These two spectrographs have contributed many of the exoplanet discoveries.) The large size, expense and long construction time has limited the number of telescopes having high precision velocimeters installed. There are many telescopes available for observing but lacking capable velocimeters, which could otherwise be participating in the Doppler planet search.

The large size and weight of a high resolution spectrograph also prevents practical airborne or spaceborne location. Secondly, infrared spectrometers must cool the entire housing to reduce thermal emission noise. The large size entails huge expense because, frequently, instrument cost is a highly nonlinear function of size and mass.

Clean instrument response needed

The spectral resolution $R = (\lambda/\Delta\lambda)$ of the spec-

trograph must be very high ($R \geq 60$ k) in order to cleanly resolve the spectral lines, which have widths not smaller than $\sim 0.1 \text{ \AA}$ at 5000 \AA , due to the rotation and turbulence of the stars photosphere. Even with this high resolution, measuring the Doppler shift of the spectrum is extremely challenging because the magnitude of the shift is 1000 times smaller than the width. Consider that the 0.1 \AA linewidth corresponds to $\sim 6000 \text{ m/s}$. Hence measuring a 1 m/s shift requires determining the change in the centroid of the measured spectral line by an amount that is 3 orders of magnitude smaller than the direct resolution of the instrument. That is, the shift is not directly perceivable by looking at the shape of the detected spectrum. It can only be done through averaging after dividing out the influence of the instrument from the data, and after careful comparison of the spectrum with a reference spectrum passing through the same instrument.

The instrument response to monochromatic light is called the point spread function (PSF). The PSF must be known or corrected for at the moment of velocimetry to a 1 part in 6000 level in order to achieve 1 m/s accuracy. The challenge is that the shape of the PSF (Fig. 3) can vary significantly (\sim a few %, implying $\sim 100 \text{ m/s}$) with environmental factors, and in a complicated way which is hard to model. The standard technique is to simultaneously use a reference spectrum. But even with a reference, significant errors can arise if the reference and starlight are treated differently, even subtly.

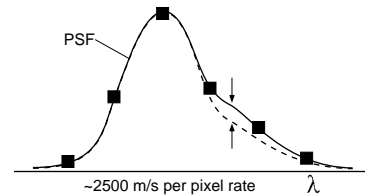


Fig. 3.— Example PSF shape (bold) and hypothetical changed shape (dashed), which could be caused by environmental insults. The large number of degrees of freedom, corresponding to the thousands of grating grooves, complicate the shape. The typical pixel spacing (squares) of $\sim 2500 \text{ m/s}$ per pixel magnifies small PSF errors into significant velocity errors.

In the currently most precise instruments, an absorptive iodine vapor cell is inserted into the starlight optical path. The iodine vapor has thousands of very narrow spectral absorption lines, which are then imprinted onto the incoming stellar spectrum. Since absorption is a multiplicative rather than additive effect, the ray path of the starlight and iodine spec-

tra are automatically wedged together, and changes in the PSF affect the stellar and iodine components similarly. But not perfectly. Since the stellar and iodine absorption lines are not perfectly co-mingled nor evenly distributed across the CCD detector, then there still remain some kinds of environmental insults, such as slight irregular spacing of the CCD pixels or air convection inside the spectrograph, that can potentially effect the stellar and reference components differently. For a typical spacing of 23 pixels per Å, which characterizes both ours and the Lick Observatory instrument (Butler et al. 1996), the velocity sensitivity to beam translational errors is ~ 2500 m/s per pixel. Hence, even millipixel distortions become relevant, and all kinds of subtle effects must be considered.

A drawback to the use of the iodine absorption cell is that it restricts the velocimetry to the 5000 – 6000 Å range (green light), because outside this range the iodine spectrum is devoid of significant features. Hence, only a small fraction of starlight photons is being used. This is especially true for red stars (M-type) which are the majority type by volume of space near Earth (Allen, 1973). These cooler stars naturally emit a majority of their photons in long wavelengths, outside the green range. To date, most stars being searched for planets are not M-type because of their faintness in the green band. A more thorough survey of all stars near Earth will eventually have to include red stars. Secondly, much interesting science will involve brown dwarfs and other low temperature objects. Hence, increasing the bandwidth, particularly toward long wavelengths, is desired.

Additive spectral references

Instead of the iodine cell, some Doppler spectrometers in use today have used an additive reference system, ie. an emission source such as a ThAr lamp whose photons are added to the starlight. The ThAr has fine lines over a much broader bandwidth than iodine, so more starlight photons can be used for velocimetry. In order to minimize the difference between the shape and position of the starlight and reference beams at the slit, which directly shifts the instrument PSF, the starlight and reference light are often scrambled together by passing them through an optical fiber. By this method precisions as good as ~ 15 m/s and 7 m/s have been reached by the CORALIE (Santos, 2000) and ELODIE (Baranne, 1996) grating spectrometers, respectively. However it

is unlikely that they will reach the 1 m/s noise level.

We propose the EDI as a method that can more accurately use an additive reference, in spite of its difficulty. And thus gaining its advantage of greater bandwidth. This has not yet been experimentally tested, since our demonstrations used the absorptive iodine cell. But we expect this because, theoretically, we find the EDI very much robust to beamshape errors. Some of the robustness comes from simple data taking stratagems that we have not yet tried.

1.2. Purely interferometric spectroscopy: FTS

An alternative spectroscopy technique that has been employed to great success primarily in the infrared region of the spectrum is interferometry, in the form of a Fourier Transform Spectrometer (FTS). This is a Michelson interferometer whose delay τ (difference in pathlength between the two arms) is scanned while the transmitted light is recorded vs τ . The measured spectrum is simply the Fourier transform of the intensity history (interferogram). The FTS is very compact, inexpensive, and insensitive to beamshape errors. Its spectral resolution can be arbitrarily precise by making τ arbitrarily long. For velocimetry of solar spectra, where the linewidths are $\Delta\lambda \approx 0.1$ Å, delays of only about 1 cm are needed. (The convenient unit of frequency for interferometry is the wavenumber $\nu = 1/\lambda$, having cm^{-1} units, and the required delay can be shown to be $\tau \sim 1/\Delta\nu$. Since $\Delta\lambda = 0.1$ Å corresponds to $\Delta\nu = 1$ cm for green light, then $\tau \approx 1$ cm.)

The serious drawback of a simple (undispersed) interferometer such as the FTS is that the photon signal to noise ratio (SNR) is very low because the crosstalk between different wavelengths all being observed simultaneously is high. The crosstalk makes the interference fringe contrast (visibility) very low, proportionately reducing the signal for a given amount of random photon noise. It can be shown (Beer 1992) that the photon signal to noise is related to $SNR \sim \sqrt{\Delta\lambda/BW}$ where BW is the bandwidth, (1000 Å between 5000–6000 Å assumed), and $\Delta\lambda$ is the effective spectral resolution needed, ~ 0.1 Å. Hence the photon noise will be ~ 100 times worse than a perfectly resolving instrument, assuming the same number of detected photons. (However, the overall transmission of a FTS is usually much higher than a grating spectrograph, so this needs to be considered.)

Figure 4 shows a comparison of estimated relative

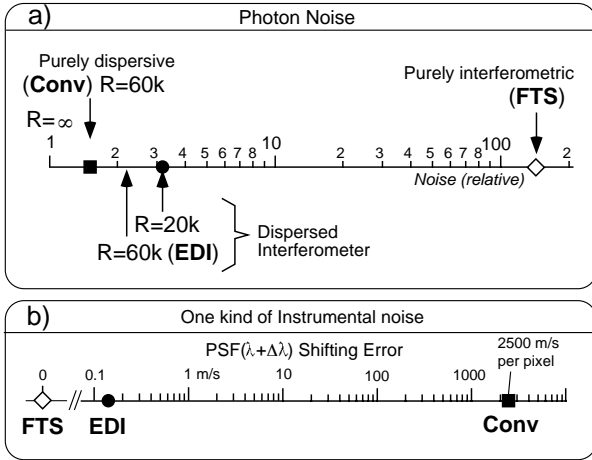


Fig. 4.— The EDI is a hybrid between purely dispersive (Conv) and purely interferometric spectroscopy (FTS), and combines the best features of both. The EDI has both low photon noise a) and theoretically low sensitivity to many kinds of environmental insults b). The FTS has poor photon signal to noise because of crosstalk between wavelength channels. Adding dispersion solves this in the EDI. The Conv is directly sensitive to errors in beamshape between stellar and reference spectra b). Adding interferometer fringes as an intermediate reference solves this in the EDI. $R = \lambda / \Delta\lambda$ is the disperser spectral resolution. The SNR for a perfectly resolving spectrograph ($R = \infty$) defines unity. The input for all methods is the solar spectrum over a 500–600 nm band. Same number of detected photons for each case assumed.

photon signal to noises for the FTS compared to dispersive spectroscopy, where the SNR for $R = \infty$ disperser resolution defines unity. The low photon noise has discouraged the use of the FTS for astronomical applications in the visible and shorter wavelengths where photons are usually scarce.

2. The externally dispersed interferometer (EDI)

Our solution investigated in this LDRD project is to combine the best features of dispersive spectroscopy with interferometry. We created a hybrid instrument, a wide angle Michelson interferometer whose output is dispersed by an external spectrograph (Fig. 5, 6). We call it an externally dispersed interferometer (EDI) to distinguish it from another hybrid instrument called the HHS (Dohi 1975, Douglas 1997) that incorporates a grating inside the interferometer. As explained later, the consequence of that is that the HHS bandwidth is severely limited, to $\sim 10 \text{ \AA}$. This prevents practical use in the Doppler planet search.

For the application of velocimetry it turns out un-

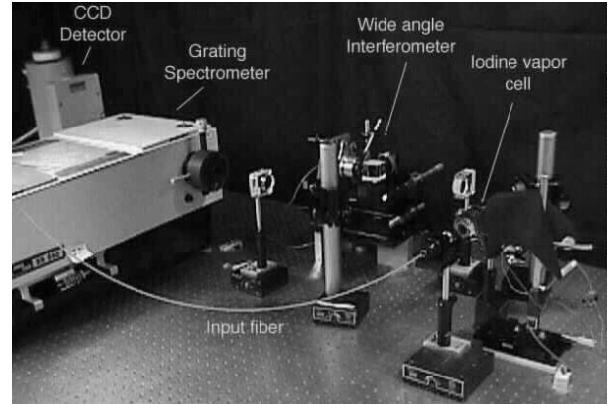


Fig. 5.— Photo of prototype externally dispersed interferometer (EDI) used for sunlight tests, assembled from off-the-shelf components. Sunlight from a roof-mounted heliostat conducted through fiber leads to an iodine vapor cell which provides reference spectrum. Wide-angle interferometer with 11 mm delay created by glass slab imprints a ladder of fringes on beam at spectrograph slit. PZT transducer increments interferometer delay in four quarter wave steps. Jobin-Yvon HR640 grating spectrograph with 0.27 \AA resolution disperses fringes into a 125 \AA spectrum recorded by CCD detector.

necessary to scan the delay as in FTS. Therefore we have limited our current investigation to an EDI with a fixed delay (dithered by a slight amount, $\sim 1\lambda$). However, some potentially useful configurations are possible with combining a traditional scanning delay FTS with a post- or pre- disperser. These have not yet been explored.

A fixed delay Michelson, having delay τ of about 1 cm, is extremely simple to construct from off the shelf components and only occupies about 1 liter of space including the mounts. Furthermore, since the delay is fixed, it is easy to use a glass slab (etalon) to virtually displace one interferometer arm relative to the other (Hilliard 1966). This creates an interferometer that, according to ray path has zero delay and is therefore angle independent, but according to time of flight has a 1 cm delay. The angle independence is a useful property that increases fringe visibility for extended sources and reduces the potential velocity error due to beam angle variations.

How it works

The interferometer has a sinusoidal transmission function T versus frequency or wavenumber (ν)

$$T(\nu) = (1/2) [1 + \cos(2\pi\tau\nu)] \quad (1)$$

shown in Fig. 7 compared against a sample of the

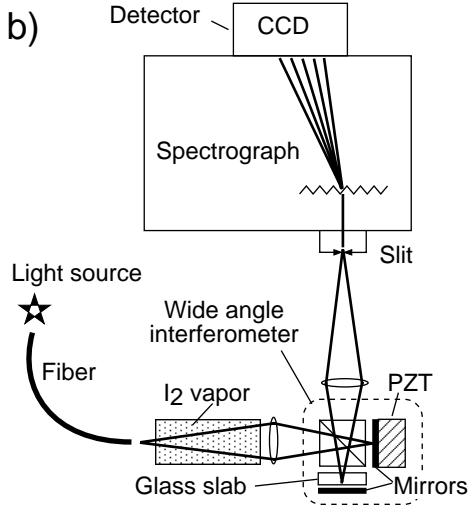


Fig. 6.— Schematic of the EDI. The cylindrical optics used to form a line-like beam cross-section in the starlight tests are not shown.

solar spectrum (representative of G-type stars). We pick $\tau \approx 1$ cm so that the periodicity of the interferometer spectral comb is 1 cm^{-1} , so that a half period (a dark fringe) matches the full width at half max (FWHM) of a typical absorption line. Since the starlight passes through the interferometer, the function $T(\nu)$ multiplies the stellar spectrum. Then any periodic structures in the intrinsic stellar spectrum $S(\nu)$ having similar spatial frequency vs. ν are heterodyned to lower spatial frequency. To avoid confusing use of the term ‘frequency in ν ’, which is a frequency of a frequency, we use the symbol ρ to represent the density of spectral features per cm^{-1} , this having cm units. Periodic structures in $S(\nu)$ have constant ρ . The variables ν and ρ are a Fourier pair.

Hence, features in the spectrum having density ρ are heterodyned to lower ρ by an amount τ :

$$\rho \rightarrow \rho - \tau$$

These heterodyned components form the Moire patterns seen in Fig. 8 and 9. We call the phase vs ν -channel of the detected Moire patterns a whirl $W(\nu)$, and this is the principle object recorded by the experiment. Let $S_0(\nu)$ be the intrinsic input spectrum before being blurred by the disperser and $s_0(\rho)$ its Fourier transform. Then it can be shown that the whirl is described by

$$w(\rho) \propto s_0(\rho + \tau) \text{psf}(\rho) \quad (2)$$

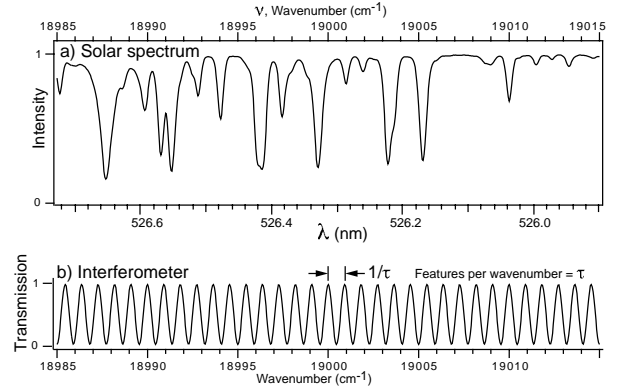


Fig. 7.— a) Solar spectrum vs wavenumber ($\nu = 1/\lambda$) or wavelength (λ). b) Transmission function of interferometer having delay $\tau=1.1$ cm, for one output arm.

where $w(\rho)$, and $\text{psf}(\rho)$ are the Fourier transforms of $W(\nu)$, and $\text{PSF}(\nu)$ respectively. The heterodyning action is embodied by the ‘ $\rho + \tau$ ’ argument. The $\text{psf}(\rho)$ factor manifests the blurring action of the disperser, which attenuates high ρ but allows low ρ to pass at unity transmission. $\text{psf}(0) = 1$ and $\text{psf}(\rho \rightarrow \infty) \rightarrow 0$. The $\text{psf}(\rho)$ FWHM is a reciprocal of the FWHM of $\text{PSF}(\nu)$.

In comparison, a conventionally recorded spectrum $S_1(\nu)$ would be

$$s_1(\rho) \propto s_0(\rho) \text{psf}(\rho) \quad (3)$$

The heterodyning action, embodied in the $\rho + \tau$ argument of Eq. 2, allows a low R disperser which can normally resolve only information at low ρ , to sense higher detail lineshape information at $\rho + \tau$. Effectively, the psf peak is moved to higher ρ by a fixed amount τ , as shown in Fig. 10a, so that it can in some ways mimic a disperser with higher resolution. The choice of τ is not critical— any value near 1 cm will do, since there is a distribution of linewidths in a stellar spectrum in this range, as seen in Fig. 10b.

2.1. Determining velocity from detected fringe spectra

It can be shown that the whirl (Moire pattern) rotates with Doppler velocity as a phasor

$$W \propto e^{i2\pi(\nu + \Delta\nu)\tau} \quad (4)$$

and

$$\Delta\nu = \nu(\Delta\text{vel}/c) = (1/\lambda)(\Delta\text{vel}/c), \quad (5)$$

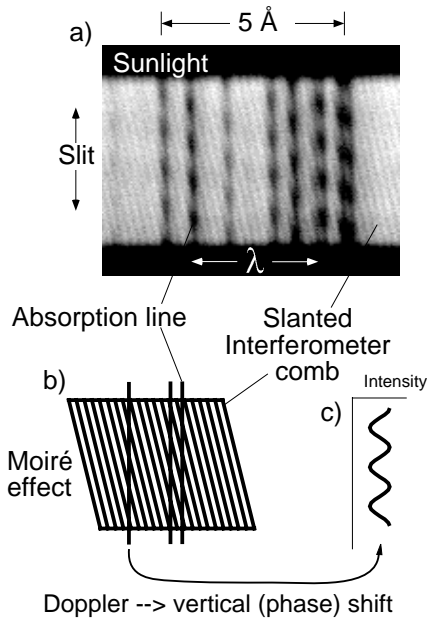


Fig. 8.— a) Snippet of solar fringing spectrum taken by the prototype EDI. The entrance slit was narrow so that the underlying interferometer comb due to the continuum can be seen. b) is model, showing moiré effect between absorption lines and interferometer comb, which creates vertically sinusoidal fringes c).

so that a rotation of 1 cycle corresponds to a Doppler velocity of ~ 15 km/s for green light. By measuring the stellar and reference spectra simultaneously, and taking the difference in rotational positions of the stellar and reference whirl components, then the velocity result is independent on the detail value of τ . Hence τ does not need to be held constant to a $1/15000$ fringe level of precision. However, wandering greater than $\lambda/4$ during the exposure would diminish fringe visibility, so we use a piggyback HeNe laser system to stabilize the interferometer cavity to gross fluctuations caused by thermal drifts and wind gusts.

The whirls can be treated as vector constructs (complex waves), and we use familiar vector operations such as inner products to compute the angular positions of the whirl components relative to pre-recorded template whirls.

2.2. Comparison to a previous hybrid system

A previous interferometric spectrometer system called the HHS (Dohi 1975, Douglas 1997) used a grating internal to the Michelson interferometer, in addition to an external one. The internal grating cre-

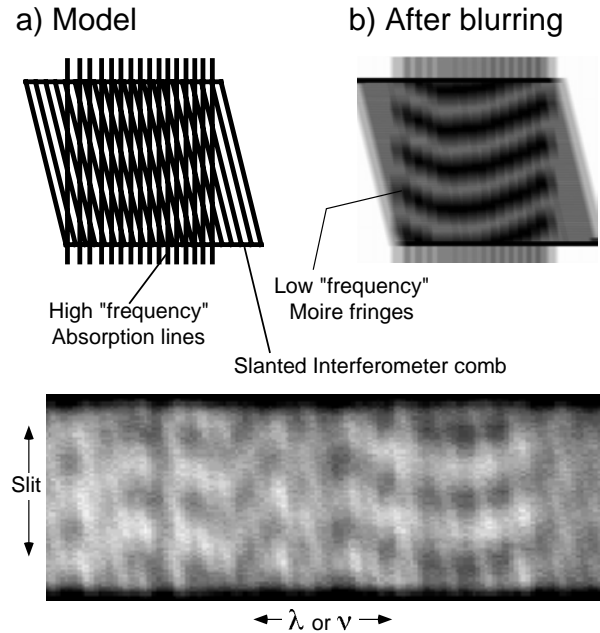


Fig. 9.— a) Model and actual iodine spectrum. a) Simulated iodine absorption lines overlaying slanted interferometer comb, without blurring of disperser, creates moiré patterns. b) After blurring of disperser the moiré fringes are still resolvable even though lines alone are not. Subtle differences in line spacing at high detail creates smile-like Moiré pattern at low detail (heterodyning effect). c) Actual iodine fringing spectrum taken with $R=20$ k disperser. Only 7 of 125 Å recorded are shown. About 1000 Å of iodine bandwidth is available.

ates differing ray angles for different wavelengths at the place of interference. Hence the fringe spacing at the CCD transverse to the dispersion axis diverges as $1/(\nu - \nu_0)$ about a center frequency. Only frequencies in a very small range are spatially resolvable by the detector pixels, limiting the bandwidth to ~ 10 Å. In contrast, the bandwidth of the EDI is not limited by the interferometer because internal to the interferometer all wavelengths travel the same path and interfere at the same angle. The dispersion is external. Hence the bandwidth is determined by choice of disperser system, which could be very wide in principle.

2.3. Heterodyning allows lower R

The fringes in the dispersion direction do not need to be resolved to measure the Doppler shift (although it can improve the SNR). This allow one to use a disperser resolution that is 3 to 10 times lower than in the conventional technique, ie. 6 to 20 k. We used $R=20$ k in our solar and labtop tests, and $R=6$ k in

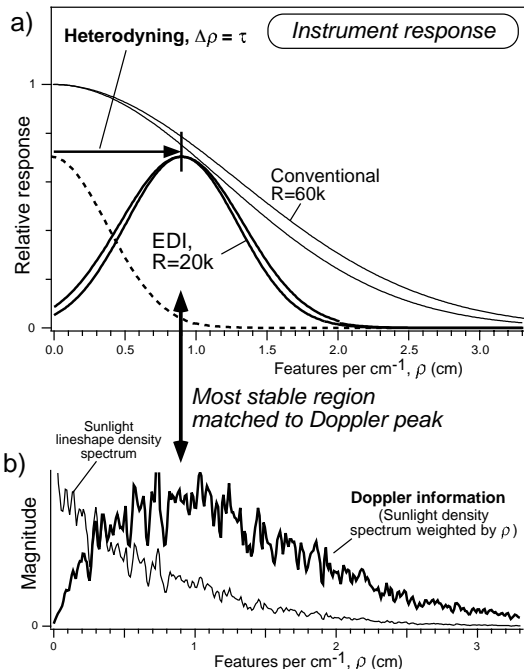


Fig. 10.— a) Instrument response vs feature density (ρ) for conventional $R=60$ k (thin curve) and EDI technique with $R=20$ k and $\tau=0.9$ cm (bold curve). Heterodyning shifts a grating response from the origin (dashed peak) to $\rho=\tau$ where its most stable region overlaps Doppler information content (bold curve of b). Doubling of curves symbolically implies sensitivity to PSF changes. b) Feature density of solar spectrum (thin curve) and Doppler content (bold). The latter is the former weighted by ρ , to manifest the $\partial/\partial\nu$ Doppler derivative. Arbitrary vertical units.

the Arcturus starlight tests.

The simulated effect of blurring in the dispersion direction is shown in Fig. 9, using the iodine spectrum (the reference we used) as an example. Fig. 9a shows the model, as if we had infinite disperser resolution. The interferometer fringe comb is slanted because τ is made to vary linearly across the spectrograph slit by tilting an interferometer mirror. Slowly varying (versus ν or λ) Moire patterns are created between the interferometer comb and the set of absorption lines, which in this example have an almost-periodic spacing near to the comb spacing. Hence the high ρ (high feature density per cm^{-1}) of the iodine spectrum is heterodyned to the lower ρ of the Moire fringes.

Figure 9b simulates the blurring action of the disperser along the ν or λ direction. Note that the original absorption lines cannot now be resolved, but the

Moire fringes can. Under a Doppler shift that moves the iodine pattern horizontally relative to the comb, the Moire fringes will move vertically, which is equivalent to a change in transverse phase. Note that the blurred Moire fringes will manifest the same phase shift. Hence, it is possible to use a very low resolution disperser to measure Doppler shift, in spite of not being able to resolve the very absorption lines that are shifted.

We find that $R=20$ k is a good compromise resolution for a disperser. It is low enough that the spectrograph can be purchased commercially and has reasonably small mass and volume, and it has high enough resolution to give a photon signal to noise that is about 1/2 of the theoretical value of a $R=60$ k conventional velocimeter system.

2.4. Increased field of view

Reducing R increases the slit opening width 3x to 10x, increasing the flux when the starlight image is blurry due to atmospheric distortions. That is, the etendue (beam area times solid angle) is increased. This is less important for the highest quality observing sites, but there are many observatories at lower quality sites with telescope time more available, and these could be used for velocimetry if a low cost system such as the EDI were used.

2.5. Increased tolerance to beamshape errors

The EDI is very much more tolerant to many kinds of irregularities in the disperser PSF affected by environmental insults, such as beamshape and beam shifting errors. This is because the interferometer comb is imprinted on the starlight in a multiplicative manner, and hence both the starlight and reference spectrum are distorted by the same amount (Fig. 7). Hence the difference between interferometer and stellar spectrum which determines the Doppler velocity, stays the same.

Because of the increased tolerance to both low R and irregular PSF, a dramatically smaller and less expensive disperser can be used and still achieve ~ 1 m/s scale precision. Figure 2 shows the dramatic difference in size between the Keck Observatory spectrometer and our prototype EDI. The several million dollar cost of the Keck spectrometer is much larger than the incremental cost of constructing an EDI.

One should keep in mind that the Keck spectrometer can perform spectral mapping in addition to ve-

locimetry, and its bandwidth is much wider than our prototype. However, the bandwidth of the EDI can theoretically be as large as the Keck spectrometer if the appropriate disperser system was used. Secondly, a variation of the EDI that uses multiple delays in the interferometer could perform mapping at very high spectral resolution. We believe that all the kinds of science measurements now being done by a high resolution grating spectrograph could be done in a competitive manner with an EDI-type of instrument.

2.6. High Photon Signal to Noise Ratio for EDI

The photon SNR of the EDI is a factor of ~ 100 larger than any undispersed interferometer technology, such as the FTS. This is because the crosstalk between spectral channels is greatly reduced. Hence, the preliminary name of the LDRD project was development of a ‘high efficiency’ interferometer, referring to the improved photon SNR. Figure 4 compares a theoretical estimation of photon noise for the 3 kinds of velocimetry techniques, for a bandwidth 5000-6000 Å of the solar spectrum (G-type stars). The EDI using a R=20 k disperser (the configuration of our prototype) has a photon SNR ~ 50 times larger than a FTS, and about a factor of 2 smaller than the R=60 k conventional spectrometer.

2.7. Robustness to beamshifting error

In exchange for the 2 times lower photon efficiency of the EDI relative to a R=60 k grating spectrometer, one gains between 100 and 10^4 times greater robustness to a variety of environmentally induced instrumental errors. One example of an important kind of insult is transverse a shift or shape change in the beam in the dispersion direction as it enters the spectrograph, as shown in Fig. 11. The conventional spectrograph is sensitive to this error at the rate of ~ 2500 m/s per pixel of shift. The EDI can be made to have, theoretically, zero sensitivity to this error, and if not exactly zero in practice, is estimated to be 10^4 times smaller.

The EDI is similarly robust to a variety of other potential insults. Some robustness requires simple modification of the instrument or data taking procedures and has not yet been tried. A demonstration of the generic robustness is the fact that we could quickly build a prototype using loosely mounted ‘breadboarded’ optics, exposed to air convection of

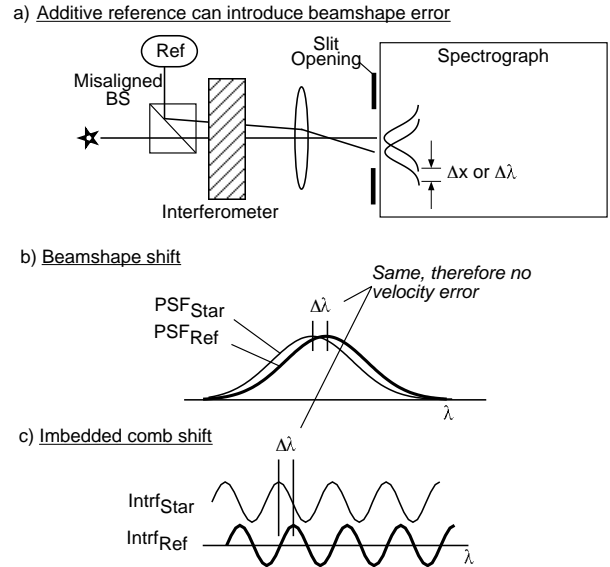


Fig. 11.— a) If an additive reference is used errors are possible that could create a relative shift in PSF position b) along dispersion direction between stellar and reference beams. For a conventional spectrometer this would create a velocity error at a ~ 2500 m/s rate. c) The EDI would have virtually no such error (smaller by $\sim 10^{-4}$) because the interferometer imprinted spectrum is carried by the light and moves with it during the error, for both star and reference beams.

the room, not temperature controlled, using off the shelf components, and still reach < 1 m/s stability over 20 minutes (Fig. 12). Whereas in order for a conventional spectrometer to reach ~ 3 m/s instrumental noise a fully matured instrument (developed over many years) in an environmentally controlled room must be used, with very rigidly mounted components.

2.8. Tradeoff between environmental robustness and photon noise

The total noise is a sum in quadrature of the photon and instrumental components. If environmental insults are severe, then the net noise performance will be instrument limited rather than photon limited. Then any method that reduces the instrumental noise is equivalent to gaining photon efficiency. Figure 13 shows how to compute the engineering tradeoff between photon and instrumental noise, where the hypothetical benefit of switching to the EDI method is a 2x increase in photon noise but a 200x decrease in instrumental noise. The conclusion is that when the exposures are long enough that one is in the instrument limited regime, then adopting the EDI can reduce the

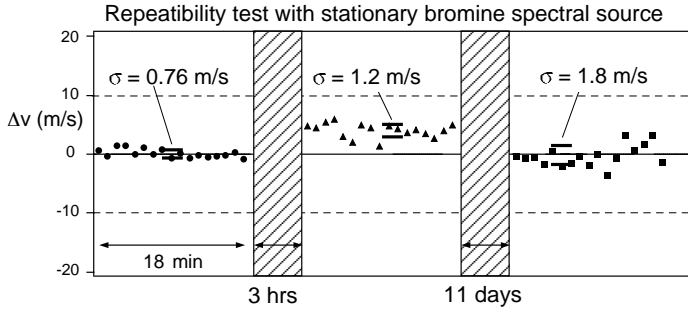


Fig. 12.— Zero velocity repeatability of the prototype instrument in the LLNL lab. A backlit bromine absorption cell is used to simulate a zero velocity Doppler source for the measurement. Short term instrument noise is <1 m/s for first 18 minutes. Here ‘ σ ’ means standard deviation. Long term (over 3 hrs or 11 days) zero point drifts were not more than 4 m/s, which is already a competitively low value compared to ~ 10 m/s noise seen in typical planet discovery data. Figure 1 shows that drifts do not exceed 8 m/s over 1 month. No environmental controls were used as would be expected in a mature instrument. Inclusion of such controls and the use of more sophisticated data taking procedures taking advantage of symmetry is expected to decrease the long term drifts to the 1 m/s level.

net noise.

What constitutes severe environmental insults? That will depend on the specific constraints that the designer faces. If cost, mass, volume or construction time are constraints, then the EDI is the preferred strategy. Simply put, it will enable quick construction of a 1 m/s capable instrument where not possible using the conventional technology. For example, it would not be possible for a project, having the same modest budget and accelerated time frame of this LDRD project, to build a 1 m/s velocimeter using the conventional grating-only technology. If cost or size is no limitation, then a grating spectrometer would be the preferred choice since that has the theoretically optimum photon signal to noise ratio.

3. Other useful variants of the EDI

For the applications of mapping and lineshape asymmetry measurement, the interferometer can have dual or multiple delays, and the values of the higher delays could be twice or three times the first delay, i.e. 2 or 3 cm. The effective spectral resolution increases proportionately with τ .

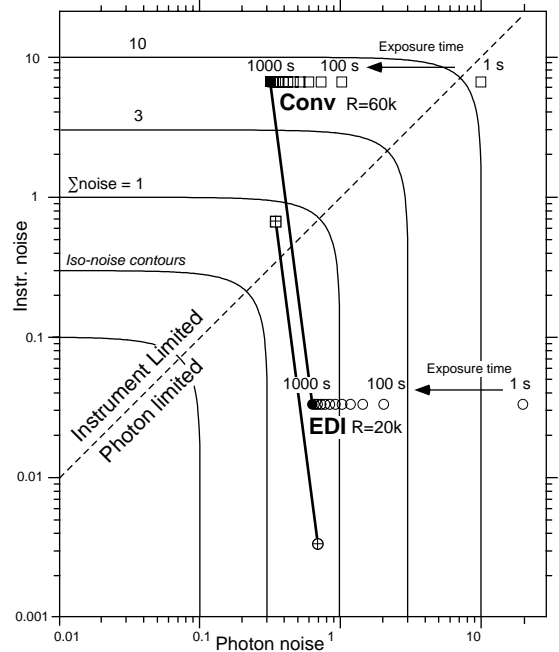


Fig. 13.— Is a 10^2 – 10^4 decrease in instrument noise worth a $2\times$ increase in photon noise? It is when environmental insults are strong. Contours of equal net noise are plotted versus instrument and photon noise contributions. Noise units are meant to be arbitrary. The logarithmic axes allow for easy scaling to the actual units, when that becomes known by the designer. Conventional method (squares) and EDI method (circles) for the same PSF insults. The theoretical benefit of EDI is a huge decrease in PSF related errors at a $2\times$ increase in photon noise (as in Fig. 4), particularly relevant when using an additive spectral reference. The EDI can decrease the net noise (solid circle compared to solid square). The breakeven case is shown with crossed circle and square.

3.1. Lineshape asymmetry using two delays

A configuration with two delays, called a dual delay EDI (DD-EDI), is useful for measuring lineshape asymmetry, which is used to measure the dynamics of a stellar photosphere. (The upwelling and downwelling plasmas have different temperatures and create an asymmetrical Doppler effect).

3.2. Spectral mapping using multiple delays

A configuration using multiple parallel delays (MD-EDI) is potentially useful for high resolution mapping, which is the measurement of the shape of an unknown spectrum and one of the most often used purposes of a spectrometer. The shared advantages of all these versions of the EDI over a conventional high resolution spectrometer is compactness, portability, inexpense,

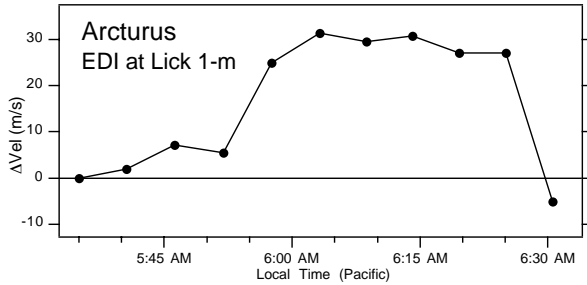


Fig. 14.— Velocity of Arcturus vs time measured using EDI prototype at Lick 1-m Observatory. Random motion of star’s photosphere is seen. Although Arcturus has no planet, the measurement tests all aspects of the system, from telescope/fiber interface to cosmic ray removal in data processing, to portability and rapid reconstruction. The spectrograph resolution was $R=5$ k here, compared to $R=20$ k for sunlight and bromine tests. Earth’s linear diurnal velocity contribution has been removed.

wide etendue (field of view), high precision, and robustness to environmental insults. The compactness is a critical advantage in infrared spectroscopy where the entire instrument and housing must be cooled to low temperatures to reduce thermal noise. The cost of an instrument is often highly nonlinear with volume. The compactness of a FTS, for example, made it a strong candidate for placement in the upcoming Next Generation Space Telescope. The EDI shares the compactness quality with the FTS.

The mathematical algorithms developed for using the EDI for velocimetry can be applied fruitfully to any combination on interferometer and external disperser. These algorithms are geometry independent and can handle irregularly shaped fringes or oddly shaped spectrograph PSF. For example, a Fabry-Perot interferometer combined with an external disperser creates circular fringes. Our algorithms can handle any geometry.

4. Summary of results

The project goal was to build a prototype EDI, demonstrate that we could detect the presence of the moon using Doppler measurements of sunlight, take the instrument to a telescope and demonstrate velocimetry on starlight.

1. Detection of Moon using Sunlight

Figure 1 shows the first milestone of detecting the moons pull on Earth. This is very relevant test because the 12 m/s amplitude velocity sig-

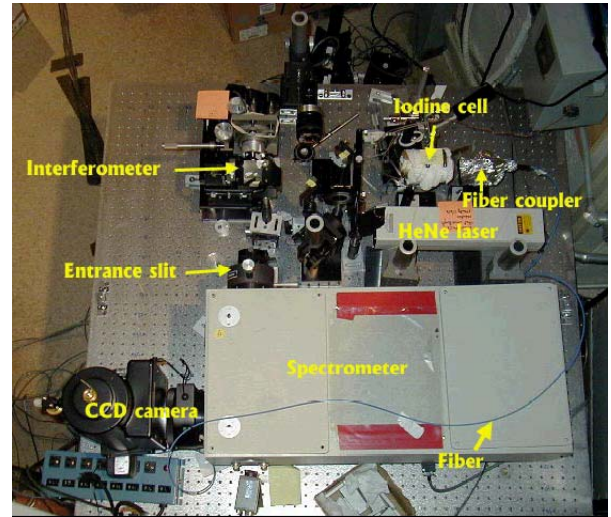


Fig. 15.— Photograph (top view) of the instrument on a 4x4 foot optical table in the Lick 1 m dome in December 1999. The apparatus differs from that in Fig. 5 by inclusion of cylindrical optics to form line-like beam cross-section (more efficient passage of starlight through spectrograph slit), and the use of a piggyback HeNe laser to roughly stabilize interferometer cavity against wind-driven fluctuations. Instrument was assembled in a few hours.

nature is the same amplitude as Jupiter pulling the sun. The 8 m/s noise in the data is not due to the EDI instrument but due to a known pointing uncertainty of our heliostat combined with a very steep (2000 m/s) velocity gradient across the solar disk. This error would not be present in stellar measurements because stellar disks are unresolved.

2. 1 m/s barrier broken

A benchtop test using a more stable spectral source (a stationary bromine lamp) should that the short term instrumental noise (Fig. 12) was less than 1 m/s, which is better than the state of the art for grating spectrometers (~ 2 m/s at best). Longer term drifts, over 3 hours, and then over 11 days, were less than 4 m/s. This is already a competitive value, and considering no environmental controls were used as would be expected in a mature instrument, we are optimistic it will be lowered after such controls and more advanced data taking procedures taking advantage of symmetry are implemented.

3. Full system test on starlight at Lick Obs.

A version of the prototype modified for obser-

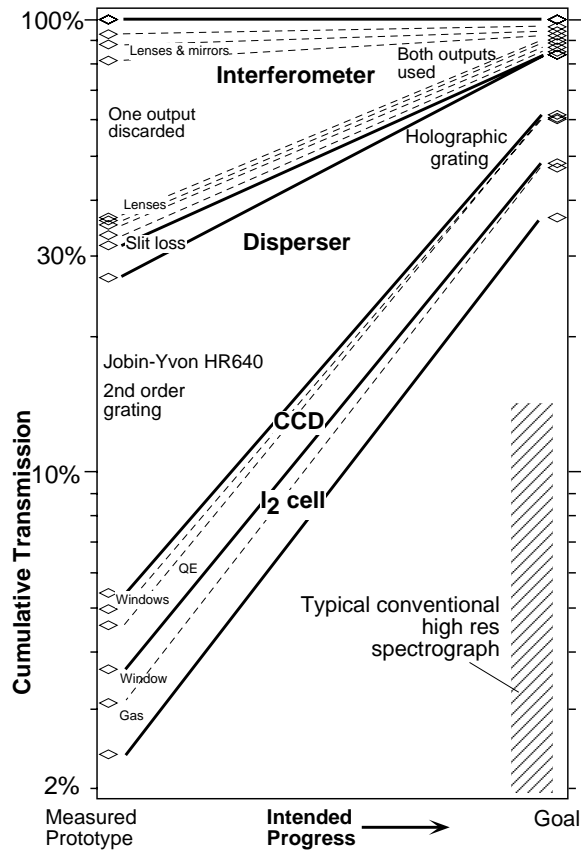


Fig. 16.— Measured and goal values of transmission through EDI prototype, after fiberoptics. Main improvements could come from using a more efficient grating and using both outputs of interferometer instead of one, doubling the transmission. Many conventional high resolution spectrographs have 5–15% transmission.

vatory operations was tested on starlight at the 1-m Lick Observatory telescope. The modifications included installation of a cavity stabilization to counter-act the drifts in interferometer delay due to temperature swings and wind-created air pressure changes. A custom designed fiber optic input system was mounted to the bottom of the telescope. Starlight was conducted to the instrument, which was on a 4x4 foot optical table (Fig. 15) adjacent to the telescope, via an optical fiber. Fringing spectra were recorded of Arcturus over a 340 Å and 740 Å bandwidth. The resulting velocity history of the 340 Å data is shown in Fig. 14. Arcturus does not have a planet and the velocity of its photosphere is dominated by random turbulence.

Arcturus was chosen because it is bright. Further work is needed to improve the conduction of light through the fiber from telescope to instrument, and replacement of the HR640 spectrograph with one having higher diffraction efficiency. The interferometer can be replaced with one using both outputs, doubling its transmission. These improvements will bring the overall transmission (Fig. 16) to a value superior than most conventional spectrographs (5–15%). The Lick campaign demonstrated that the entire EDI system, from telescope, to instrument, to data processing algorithms was functional. The instrument was disassembled, moved and reassembled in a few days, thus proving the rapid re-construction time and portability of the instrument.

5. Summary of benefits

In comparison to the **FTS**, the EDI

1. Is much more efficient in low light level applications where photon noise dominates
2. Can operate with no moving parts and therefore record single-shot events (e.g., diagnostics of explosions).

In comparison to a high resolution ($R=60\text{ k}$) **grating spectrograph**, the EDI

1. Is much smaller, lower weight and therefore can be put on airborne or spaceborne platforms where previously not practical.
2. Is theoretically much more robust to a variety of environmentally induced errors, further reducing cost.
3. Can use a 3x to 10x lower resolution grating, and tolerate optics with greater aberrations. This can only improve the transmission of the overall instrument (and thereby reduce photon signal to noise) by allowing the designer to choose components optimized for efficiency instead of tight and uniform PSF. For example, diffraction limited holographic gratings having near ideal efficiency could be used, whereas previously they may have been avoided due to an irregularly shaped PSF.
4. Can be rapidly built using off the shelf components.

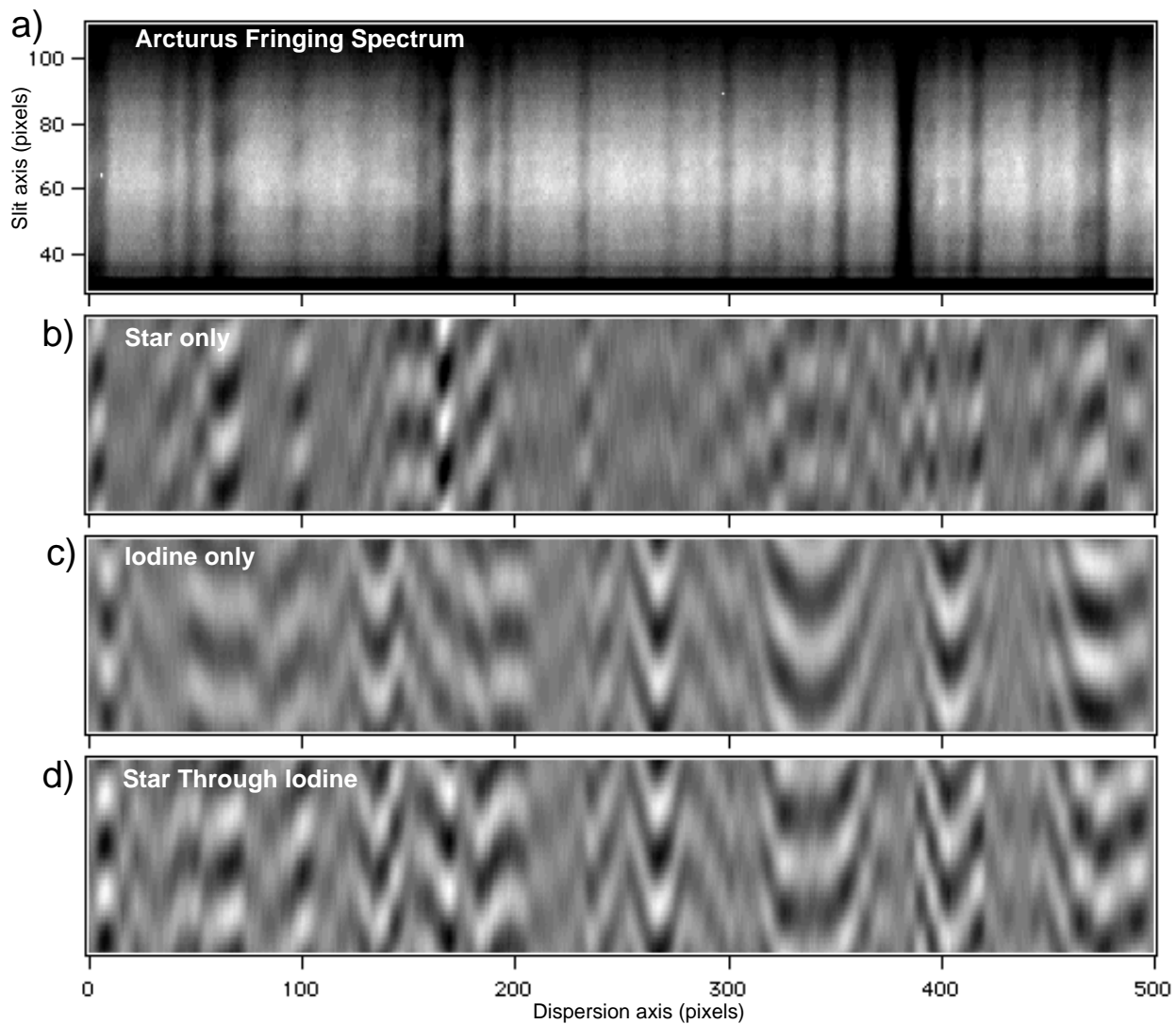


Fig. 17.— Set of fringing spectra data, raw and processed of bright star, Arcturus, taken by the fiber-fed EDI in December 1999. Fringe contrast is lower here than in bromine-iodine test due to lower spectral resolution ($R=5.6k$ vs $R=20k$). Only 70 of 340 Å recorded bandwidth is shown. a) Raw fringing spectrum showing moiré fringes. b) Processed version of data in a), after removal of nonfringing components along vertical axis. This *Star* whirl was used as a template. c) *Io* whirl template taken of white light passing through iodine cell. d) Example of many *StarIo* whirls taken of Arcturus starlight passing through iodine cell. Each *StarIo* whirl yields a velocity datum when the rotational angle between *Star* and *Io* components is determined through application of dot products against the templates.

5. Portable.
6. Wider field of view increases photon flux for extended objects, such as stars blurred by the atmosphere.
7. Has a demonstrated velocity precision which already approximately matches the state of the art and is likely to exceed it with further development.

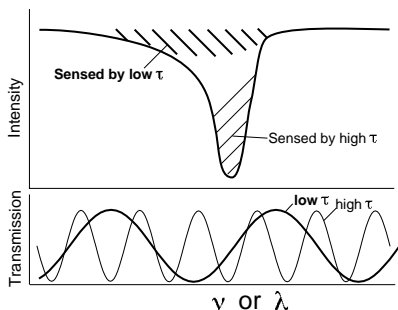


Fig. 18.— Lineshape asymmetry due to photosphere dynamics can be probed using two parallel interferometer delays having widely different values, so that the corresponding spectral combs have different periodicities. These sense different portions of an asymmetrical absorption line. The same disperser could be used for both delays to minimize common mode errors. Changes in asymmetry then manifest a differential Doppler velocity. The asymmetry here is greatly exaggerated for clarity.

Science and technology benefits

1. For the Doppler Planet Search

Increase the number of telescopes having 1 m/s capable spectroscopes, by lowering their cost, weight, time to build, relaxing tolerances on grating resolution by 3 times, greater bandwidth by allowing use of additive spectral references, much more tolerant to beamshaping errors. Greater tolerance to optical irregularities could allow use of more efficient diffraction gratings, removal of pupil masks, widening slit openings, and other pro-efficiency choices.

Greater velocity precision allows detection of lighter mass planets and improves detection of companion planets in multiple planet systems, and long period planets observed over partial orbits.

2. Other velocimetry

Asteroseismology. Improved velocity precision and more transmissive instruments would allow time resolved velocimetry of the stellar photosphere, called asteroseismology, which can probe stellar interiors and help distinguish photosphere motion from planet pulling.

Asteroid orbits. Improved and more rapid determination of the orbits of asteroids or other sunlit bodies using radial velocity. Currently, only the apparent transverse motion is observed, and this requires observation on two or more successive nights. The third component, being the radial velocity, is not now measured due to the expense, and therefore rarity, of high resolution grating spectrometers. The radial velocity information can improve upon the accuracy of the predicted orbit characteristics, and it requires only one night of observation. For some places in the asteroid orbit (such as on the opposite side relative to the sun) the radial velocity component alone can mean the difference between hitting or missing the Earth.

Passive Satellite Ranging. Passive (surreptitious) determination of closing velocity of a target, such as between one Earth orbiting satellite and another, using natural sunlight. Previously, spacebased use of high resolution spectrometers was prohibited due to their large (5-meter) size and great mass. Passive probing has advantages of not alerting the target to ones intentions, and not requiring a high energy source to power the illumination.

3. For Lineshape Asymmetry

Measurement of lineshape asymmetry is a method of studying the dynamics of stellar photospheres. A dual delay version of the EDI that could measure lineshape asymmetry is estimated to have 3 to 10 times greater photon signal to noise than a R=60 k conventional spectrometer. This is because the $\text{psf}(\nu)$ of a conventional spectrograph falls off exponentially or faster at high ρ , whereas for it does for the EDI, because the heterodyning action effectively shifts the psf peak to high ρ by amount τ . Figure 18 shows how the different delays (here in a 3:1 ratio) sense different portions of the line. Once computes the velocity of each section. A difference in velocity between pedestal and peak indicates asymmetry.

4. For Spectral Mapping

Measuring the shape of an unknown spectrum (mapping) is one of the primary uses of spectroscopy, throughout science, and for remote sensing in national security. A multiple delay version of the EDI is estimated to have better photon SNR for mapping when measuring very high detail ($\rho > 2$ cm). This would dramatically reduce the size and cost of high resolution spectrometers. In comparison to FTS spectrometers, which now fill this niche, the EDI does not scan its delay over time and therefore can measure single-shot events that a FTS cannot. The lack of moving parts may make installation in remote sites such as the Next Generation Space Telescope attractive.

5. For Metrology

Our demonstration of 0.76 m/s short term velocity repeatability (Fig. 18) for a stationary input spectrum, which appears to be photon-limited, implies the instrument noise is better than $\sim 1/20000^{th}$ of a wave, or 0.025 nm. This is an order of magnitude better than most other fringe shift technologies, which are in the $1/1000^{th}$ wave range. Secondly, we can unambiguously determine absolute distance to a precision of 1 part in 3×10^8 . Hence there is no possibility of fringe skip error, as in monochromatic systems. Precision sensors could be built where a secondary effect such as temperature, acceleration, magnetic field etc. is measured through its effect on the interferometer delay, through either a moving mirror or change in refractive index of a medium.

The key is the use of polychromatic instead of monochromatic light. Having N multiply independent channels with unrelated phases statistically reduces the systematic errors by $1/\sqrt{N}$. Since N can be ~ 1000 , this allows us theoretically to reduce the systematic noise, which is the limiting factor when sources are bright, to more than an order of magnitude below that of monochromatic or equal-pathlength systems, which is the way such measurements are now performed.

Due to the limited duration of the project only the Doppler velocimetry applications have been demon-

strated in experiments. The other potential applications remain to be developed.

Part II

A More Technical Description, focusing on Observatory tests

6. Introduction

Radial velocity precision is limited by a combination of factors: instrument noise, photon noise, and intrinsic stellar photospheric activity. Instrument noise is essentially determined by the ability to determine the point spread function (PSF) in effect at the moment of observation with sufficient precision, since this can wander with time due to environmental factors. Since a desired 1 m/s precision is approximately 5000 times smaller than the width of narrowest stellar spectral feature, exceedingly small changes in the centroid of the PSF become important.

The uncertainty in the PSFs of current echelle grating spectrometers produce errors at the 2 m/s level (Butler et al. 1996). Fundamentally, a grating PSF is formed by the interference among thousands of grating grooves, and hence a multitude of free parameters potentially belong in the PSF model. Thus practical models which employ smaller number of parameters can lead to slight but significant errors in the PSF centroid location.

Photon noise is an important contribution to the net noise, and is straightforwardly determined by the number of photons that successfully pass through the spectrometer and reach the detector, by an inverse square root dependence. Given a fixed size of telescope diameter, it is desired to maximize the efficiency of the spectrometer system, which includes minimizing light excluded by the slit at the spectrometer entrance, maximizing diffraction efficiency of the grating, and minimizing any masking of the pupil used to create a more uniform PSF. There are engineering trade-offs between the width and uniformity of the PSF and the consequent efficiency. For example, a narrower slit decreases the PSF width while excluding photons from blurry star images. Efficiencies of current planet seeking spectrometers are not better than several percent when operated in the high resolution mode needed for Doppler measurements. This conclusion is based on the reported exposure times re-

quired to achieve a given signal to noise ratio (SNR) (Butler et al. 1996). Hence there is room for significant improvement in this area, which will directly improve the rate of surveying thousands of stars for planets.

The third source of error is due to the motion of the star's photosphere. Recent analysis of Lick echelle spectra by Saar et al. demonstrate that most stars appear to have some magnetic related radial velocity noise at the level of at least a few m/s (Saar, Butler & Marcy 1998). However, this is not a firm velocity boundary, because in principle some of this activity is due to regular oscillations of the photosphere, which could be modeled and removed from the net velocity signal if the measurements were sufficiently time resolved. Current instruments have not yet demonstrated the ability to time resolve the oscillations (other than our sun) due to their low efficiency and high instrument noise. This limitation can be surmounted with present size telescopes if instrument efficiency is optimized and instrument noise greatly reduced. Furthermore, the ability to time resolve photosphere dynamics is scientifically valuable in its own right, since it allows study of the interior of the star through the careful measurement of the frequency distribution of the normal modes of oscillations, as has been well-demonstrated with our sun (helioseismology).

7. Externally Dispersed Interferometer concept

We report a new kind of instrument for measuring 1 m/s scale Doppler shifts of broadband light which has low instrument noise and has the potential for great efficiency. Compared to current Doppler spectrometers, this instrument is compact, inexpensive, and can be assembled from off-the-shelf components. It is called an externally dispersed interferometer (EDI), or previously (Erskine & Ge, 1999), a fringing spectrometer. It is a series combination of a Michelson-type interferometer and an intermediate resolution spectrograph. The interferometer is responsible for the Doppler shift measurement by creating fringes through two-beam interference. A Doppler shift manifests a phase shift of the fringes. Because all wavelengths travel through the same optical path through the interferometer, the spectroscopic behavior (instrument transmission function or PSF) is extremely regular versus frequency, being a sinusoid

with only 3 degrees of freedom: phase, amplitude and offset. Many environmental insults which would affect the PSF of a grating do not change the functional character of the interferometer response. For example, a hypothetical change in the reflectivity of an internal mirror surface due to corrosion or condensation will alter the phase, amplitude or offset of the sinusoid, but the response will remain a sinusoid. This allows the data analysis to be robust against many kinds of drifts.

An alternative but related explanation of the advantage of the interferometer invokes the Moire effect (Fig. 8). The sinusoidal transmission function of the interferometer multiplies the input spectrum. The half-period of the sinusoid is chosen to match the typical stellar absorption linewidth. The multiplication by a sinusoid heterodynes high detail spectral information which contains the Doppler shift information to low spatial frequency (along the dispersion axis). It is easier for the spectrograph to accurately measure low spectral detail than high detail.

Furthermore, because of the heterodyning, the required PSF width to resolve the moire fringes can be 3x-10x coarser than a grating-alone instrument. In lab tests with our prototype we have demonstrated that a slit width of 0.27 Å suffices to reach the 1 m/s precision regime instead of the ~ 0.08 Å maximum width required of current Doppler spectrometers. This allows the net instrument efficiency to improve for several reasons. 1) The wider slit allows more light from a blurry star image to enter the spectrograph. 2) The instrument is insensitive to PSF non-uniformities. This allows pupil masks to be removed. 3) The size and expense of the grating can be reduced greatly. This allows the use of alternative grating technologies such as holographic gratings. These gratings can be optimized for maximum diffraction efficiency at the expense of poorer PSF, since the tolerance for PSF is now greatly relaxed with our scheme. For example, commercial volume holographic gratings are available which are 80% efficient to unpolarized light (Kaiser Optical Systems, Ann Arbor, MI).

Currently our interferometer only uses one of two available outputs. However, we plan use interferometers which direct both outputs to the detector so that the interferometer insertion loss is much closer to unity.

Why include a grating at all? The inclusion of the spectrograph increases fringe visibility by prevent-

ing crosstalk between fringes belonging to neighboring spectral lines, which are typically separated on a 1 Å scale. This increases the signal to noise over an interferometer used alone with broadband light, such as a Fourier Transform spectrometer. This SNR issue has previously limited the use of undispersed interferometers to applications which are not photon limited.

The combined use of interferometry with dispersive spectroscopy is a novel approach that is unfamiliar to both dispersive-only and interferometer-only instrument communities. This required us to build new mathematical tools for manipulating spectra having thousands of parallel channels containing independent fringes. Our strategy for development of the hybrid instrument has been to first build, demonstrate and explore the velocimetry aspects of the technology while postponing installation of transmission efficiency increasing aspects. This allowed us to develop the fringe shift data analysis software using actual fringing spectral data, obtained with bright convenient sources, and to most rapidly demonstrate the most challenging aspect of the project: reaching 1 m/s velocity precision while using off-the-shelf equipment.

Initial tests on bright sources including sunlight, bromine absorption cell and bright stars ($V=0-1$) confirm that the fundamental velocimetry aspect of the new optical technique works and can reach <1 m/s short term instrument noise using off-the-shelf components. Using the bromine absorption spectrum as a convenient and quiet constant velocity source, we find that with a 0.27 Å slit width ($R=20$ k) we can achieve 0.7 m/s total short term noise (which includes photon noise). Longer term drifts on a several m/s scale are expected to reduce after we identify their origin (the instrument was open to the air, the interferometer cavity unstabilized, and the bromine temperature/pressure was unregulated). From our initial experience with star light under observatory conditions and 1 Å slits ($R=5.6$ k) we conclude that the maximum practical slit width to achieve the 1 m/s precision regime is closer to 0.27 Å than to 1 Å. Future star light observations using a 0.27 Å slit are expected to reproduce the 1 m/s precision regime seen in lab tests. Our star light tests will resume after we modify the prototype to operate more efficiently at narrower slit width.

8. EDI technique

The dispersed interferometer technique is based on the moire effect. This occurs between the sinusoidal frequency response of the interferometer (fringe comb) multiplied against the absorption or emission lines of the input spectrum. A small segment of dispersed interferometric fringes of the solar spectrum is shown in Fig. 8a, taken with slits narrow enough to resolve the interferometer comb. The comb half-period (0.13 \AA) is set to roughly match the typical absorption linewidth. The comb is slanted by tilting interferometer cavity mirror so that the fringe phase varies along the slit length.

As modeled in Fig. 8b, the overlay of the comb with the solar absorption lines creates moire fringes having sinusoidal character in the direction along the slit (Fig. 8c). These fringes will move along the slit direction (vertically) under a Doppler shift. Hence we measure the Doppler effect by a transverse shift of the fringing spectrum, instead of measuring the horizontal (dispersion axis) shift of the spectrum as in a conventional spectrometer. The fringe phase and amplitude for each wavelength channel is determined during data analysis from the sinusoidal intensity dependence, either versus position along slit length and/or versus interferometer delay in a phase stepping procedure using several exposures incremented by 90° phase steps.

In principle, any number of spatial fringes can be used along the slit, but best signal to noise is obtained when the spatial frequency is maximally different from the dominant spatial noise, which may be due to CCD pixel to pixel gain variation. We find having 4 to 6 fringes across the beam, which occupies 60-80 pixels along the slit, is effective in our prototype. (Hence we are only utilizing 10% of the available height of the CCD chip [600x2500]). In this configuration the slit is a narrow rectangle. Hence for efficient use of light the round input beam should be converted to a rectangular cross-section. This was accomplished in our later prototype by cylindrical optics, but could also have been done using image slicing.

In future applications of our technique, we anticipate that a desirable disperser may be a cross-dispersed echelle grating system, because this type provides wide bandwidth at good resolution, and greatly reduces the need for image slicing. Since this kind of disperser has a more square-like slit opening, the number of fringes across the slit would be chosen

to be small, such as two, one or zero. By zero we mean essentially an infinitely wide fringe (no slant in the fringe comb). In the case of infinitely wide fringe, the phase for a given wavelength channel cannot be uniquely determined from a single exposure, but can be determined through the phase stepping procedure, which we typically apply in any case to improve rejection of common-mode noise.

Similar to conventional Doppler techniques, a spectral reference source is required to provide an accurate absolute zero for the dispersion and phase (slit) axes. This can be either an absorption spectrum, such as the popular iodine vapor cell, or an emission source, such as a thorium lamp. Absorption references are preferred because they imprint their spectral information through a multiplicative rather than additive process, so that all rays will be modified the same way independent of ray direction.

A drawback of the iodine cell is that it is limited to the green wavelengths. This fact has limited current Doppler searches to stars which are brightest in the visible, and largely prevented use on M dwarf stars. This is unfortunate since these dwarfs constitute a majority of nearby ($d < 8 \text{ pc}$) stars (Henry 1991). However, these are too faint ($V \approx 11$) to be efficiently observed with current optical echelle at the largest telescopes such as the Keck 10m.

Since these stars are about 10 times brighter in the near-IR (Kirkpatrick et al. 1993), there is strong motivation to develop Doppler spectroscopy techniques for this wavelength region. Our interferometric technique is such a viable method.

9. Implementation of an EDI

9.1. A prototype for lab experiment

In order to demonstrate the concept for this new approach, a prototype dispersed interferometer was quickly assembled in 1998 using commercially available optics, an existing commercial spectrograph (Jobin-Yvon HR640) and a 2500x600 CCD camera with $12 \times 25 \mu\text{m}$ pixels (Princeton Instrument). It was a bench mounted instrument in a lab at LLNL (Fig. 5). A fiber with 1 mm diameter was used to input light from emission line and continuum lamps, HeNe lasers and solar light. The interferometer is a Michelson type with an approximately fixed but adjustable delay of about 11 mm (not scanned over large delays as in a Fourier Transform instrument). A 50/50 BK7 beamsplitting cube was used to split the incoming

beam into two beams which nearly retro-reflect back from the interferometer mirrors. One beam was further delayed by a 6.3 mm BK7 etalon, so that the virtual image of the two mirrors superimpose longitudinally. This produces an angle independent delay. The two reflected beams interfere with each other in the output to form fringes versus both frequency and (optionally) spatially. Tip/tilt control on one mirror adjusted the spatial fringe density to the desired value, which was typically 4-6 fringes across the beam at the slit. A PZT pusher was attached to a mirror to provide piston motion. This linear motion control is critical for stepping the delay by quarter wave increments in several exposures. This phase stepping is used to isolate actual fringes from beam profile variations which could be confused as fringes. Only the true fringes will have the expected sinusoidal dependence.

The interferometer and spectrograph were operated at $f/18$. The image size at the spectrograph entrance was about 2.4 mm in diameter. An adjustable slit was used for the experiments. A $70\ \mu\text{m}$ width was set for most of the lab testing to provide a spectral resolution of $R \approx 20,000$ with a 1200 l/mm grating operated in the 2nd dispersion order at $5400\ \text{\AA}$. The full wavelength coverage with the CCD detector was about $124\ \text{\AA}$. Fig. 8 shows a small portion of the solar spectrum taken with this prototype.

This prototype was used for the lab experiments until April 1999. Some preliminary results were reported in a previous conference proceedings (Erskine & Ge 1999). For expediency, no cylindrical optics or means for converting the round input beam cross-section to a rectangular shape was employed. Hence only a few percent of input light entered the slit, and we were limited to bright sources with this first version of the prototype.

However, the experiments conducted with this prototype were extremely useful in exploring the fundamentals of velocimetry using this new technique, providing us with early fringing spectra data with which we could validate the developing data analysis algorithms.

9.2. A fiber-fed EDI

In April of 1999 we began designing modifications to the first prototype to facilitate initial tests on starlight at the Lick 1m telescope. These modifications involved 1) adding cylindrical optics to convert

the round input beam to a rectangular cross-section to more efficiently fit the beam through the slit; 2) construction of a fiber optic feed at the Cassegrain telescope focus; 3) active stabilization of the interferometer cavity to allow long time exposures coordinated with phase stepping; and 4) reassembly of the prototype on a small breadboard which can easily be relocated to the observatory.

Fiber feeding was chosen to easily couple the instrument with the telescope. The instrument can also be located at a convenient place for the testing. The instrument stability can also be improved by separating the instrument from the telescope.

The optical layout was designed with a commercial ray tracing software, ZEMAX (Focus Software, Inc.). The layout included fiber-feed, interferometer and spectrograph subsystems. The Jobin-Yvon Inc. spectrograph was modeled as a standard a Czerny-Turner design without optimizing any of spectrograph optics.

Figure 19 is a photograph of the fiberoptic/telescope interface installed at the Cassegrain focus of the Nickel 1m telescope at Lick Observatory. It includes a field lens located at the telescope Cassegrain focus to form a telescope exit pupil. A reimaging lens changes the telescope $f/17$ beam to a $f/20$. A pinhole with a shining aluminum surface was placed at the new image plane. The surface reflects the light to a commercial Cohu CCD camera to help to find the target stars within the 40 arcsec field of view. It was also served to monitor the star image for guiding during the exposure. The $f/20$ beam was converted to $f/4$ by a small achromat, and then entered a fiber with $70\ \mu\text{m}$ diameter (3.6 arcsec on the sky).

The optical layout of the interferometer and spectrograph on the table is shown in Fig. 20. Fig. 15 is a photograph of the instrument at the Lick 1m observatory. The interferometer subsystem includes a beam splitter with a BK7 glass etalon, a fiber output coupler (L1), a cylindrical lens (L3), field lenses (L2, L4) and a reimaging lens (L5). The cylindrical lens (L3) converts a circular image from the fiber output to a rectangular one at the mirrors M1 and M2 where the fringes can be considered to form. The operation of the interferometer is similar to that in the prototype. The rectangular beam is splitted equally by the beam-splitter. One beam is reflected directly from mirror M2, the other is delayed by the BK7 etalon with 6.3 mm thickness before reflecting back from mirror M1. The two beams interfere with each other and form a

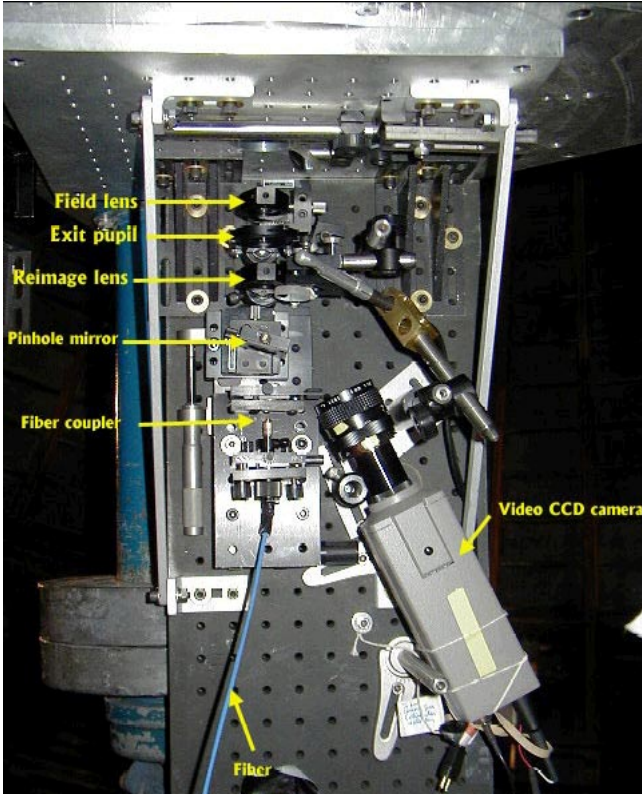


Fig. 19.— Photograph of the fiber feed at the focal plane of the Lick 1m telescope in December 1999. The video camera views a small metal disk with a pinhole through which the starlight must pass, so that we can see when the telescope is mis-pointed and judge the degree of focus.

ladder of spatial fringes which are superimposed on the slit by reimagining lens L5. The field lens L4 keeps the pupil within the aperture of L5. The image on the slit had a size of $140 \times 2000 \mu\text{m}$. Monochromatic light from a Hg lamp created a 7 pixel ($84 \mu\text{m}$) full width at half maximum (FWHM) peak on the CCD when the prototype was at Lick.

In order to increase flux, the 1200 1/mm spectrograph grating was switched from the 2nd order configuration used in lab tests to the first dispersion order. This provided $R \approx 5600$ at 5400 \AA and 340 \AA wavelength coverage. However, the consequence of the wider slit was that the underlying interferometer fringe comb (Fig. 1a) could no longer be resolved, and there was increased crosstalk between adjacent channels of the remaining Moire fringes. These two effects were later determined to be responsible for most of the observed decrease in signal to noise ratio. We expect that returning the spectrograph to a resolution

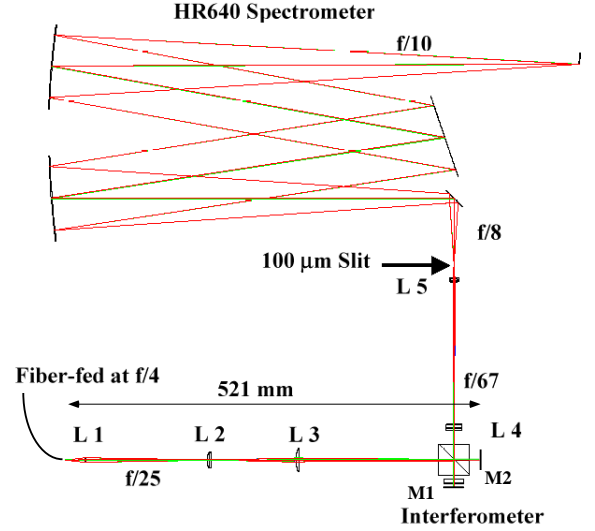


Fig. 20.— Optical design of the fiber-fed EDI.

of $R=20000$ will reproduce the 1 m/s precision seen in the lab tests.

The alignment of the fiber feed at the telescope was conducted in the following procedure. We first align the telescope pupil to the exit pupil, then adjust the location of the pinhole until the image fills it. We then apply a HeNe laser beam backward from the instrument bench to align the laser beam with the pinhole and then let the beam fill the exit pupil. The alignment of the interferometer and spectrograph is relatively easier and less critical than that for the fiber feed.

9.2.1. Throughput

Figure 16 shows an estimated an element by element breakdown of the power loss through our prototype when it was in the fiber fed configuration immediately prior to being relocated to Lick observatory, with the exception that the grating was still in the 2nd order configuration (greater diffractive loss). This is transmission of power through the system, per unit bandwidth, after the telescope.

Measurements were made both of individual elements and groups of elements, using collimated green HeNe light, green incandescent light and a power meter at various positions along the optical train. In some cases the individual throughput values for elements were modified so that the product of their values agreed with measured integral values. The re-

sulting throughput breakdown is shown on the left side of Fig. 16.

The right side of that Figure is an estimation of what could be achieved in the long term, by substituting more light efficient (AR coated) or higher wavefront quality components, eliminating unnecessary surfaces, using both outputs of the interferometer etc. There is available a large room for improvement of approximately 30x, which would bring the total efficiency to 30-40%. If successful this would be a significant advance over the state of the art. Some losses are common to all Doppler spectrometers, such as the CCD detector quantum efficiency and the iodine cell. The fiber losses could be eliminated if the fiber was not used as a delivery system, since the small size of our instrument allows it to be mounted directly on the cassegrain focus of most telescopes. The Keck and Lick echelle spectrographs do not use fiberoptic delivery for example.

The throughputs (losses) of the prototype can be grouped into three subsystems: fiberoptic delivery system between telescope cassegrain focus to the interferometer, the optics in the vicinity of the interferometer including the cylindrical beamshaping optics and relays to the spectrograph, and the spectrograph. The losses from the iodine cell and its two uncoated windows was considered separate from the interferometer, even though it was physically adjacent.

For the fiberoptic subsystem there are parasitic reflections off the lenses preceding the fiber, loss through pinhole, coupling loss at the fiber entrance, and an effective loss due to the unwanted growth of the numerical aperture of the beam leaving the fiber beyond the $f/4$ design value. (That value runs up against the $f/8$ acceptance limit of the spectrograph and the 2x magnification of the intervening optics). We found that although we could initially achieve an $f/4$ beam out of the fiber, this could degrade to $f/3.2$ with typical handling due to stress on the fiber chuck. Improvements to this subsystem including using stress-free fiber chucks, anti-reflection coating of the lenses, the possible elimination of some lenses and the pinhole, and the use of larger diameter fibers (discussed below).

For the interferometer, there are parasitic reflection losses due to uncoated optics. These can easily be reduced by AR coatings. But the chief present loss is the discarding of one of the two interferometer outputs, the one that travels nearly backwards off the interferometer mirrors toward the source. This rep-

resents an immediate 50% loss. However, in principle an interferometer can be designed which routes both outputs in the same general direction, so that both outputs reach the CCD chip. (One wants them to be slightly displaced from each other on the chip by an odd number of half waves, so that they combine to increase the fringe contrast.) This would improve the throughput of the interferometer by a factor of up to 2x.

For the spectrograph subsystem, the throughput is dominated by the grating diffraction efficiency. At the time data for Figure 16 was measured the grating was used in 2nd order, and the net throughput of the HR640 spectrograph was only 20%, which was disappointing. Consequently after we relocated the prototype to the Lick Observatory we switched the grating to 1st order. We did not measure the new diffraction efficiency, but it may have improved it to 40%.

The spectrograph diffraction efficiency can be greatly improved by use of volume holographic gratings. We have such a grating (Kaiser Optical Systems, Ann Arbor, MI), and its advertised efficiency is 80% for unpolarized light. It is also an attractive spectrograph because its bandwidth is nearly the 1000 Å needed to cover the iodine spectral range in the green, and the numerical aperture of the spectrograph is extremely fast, $f/1.4$. The latter creates an available etendue of 900 micro steradians square cm, which we estimate is two orders of magnitude greater than that of the Hamilton spectrograph at Lick. If an image slicing method is used to convert the round beam into a narrow rectangle, this extra etendue could be used to accommodate an order of magnitude larger diameter fiber, which would reduce loss at the pinhole due to blurry star images.

9.2.2. *Other flux or speed affecting factors*

Larger fibers. The throughput could increase from the use of a larger diameter fiber, both because the tolerances on the numerical aperture and diameter of the fiber would be more relaxed, and because it could accommodate a star image meandering due to uncorrected atmospheric turbulence. The diameter could be increased if an etendue-conserving image slicing scheme was employed to efficiently convert the large available rectangular area of the slit (84 x 15000 μm @ $f/8$) into a circular cross-section. The present cylindrical optics system both uses only 13% of the available height of the slit and secondly does not

conserve etendue (cross-section times numerical aperture). A fiberoptic bundle is one suggested means of converting the beam cross-section shape. The full 84 x 15000 μm @ f/8 slit area could create a circle of diameter 22 arcsec diameter on the sky with the HR640 spectrograph. Even larger etendues would result from use of the holographic grating. These large instrument etendues could be used to good advantage in accepting light from a farm of inexpensive telescopes, which could lack adaptive optics and be located at sites with less than ideal seeing to save costs.

Bandwidth. The net flux reaching the detector is proportional to the bandwidth of the spectrum used. With our present grating used in either 1st or 2nd order we had bandwidths of 343 \AA and 124 \AA respectively. We also took fringing spectra at 740 \AA using a coarser grating, but did not process these into velocities. Hence we demonstrated that the bandwidth is not limited by the interferometer, and is simply due to choice of disperser. Increasing the bandwidth to the 1000 \AA (5000 - 6000 \AA) bandwidth of iodine would boost the flux by factors of 3.5x and 10x, respectively.

Fringe contrast. The signal to noise of our instrument is proportional to its fringe contrast ability. Hence it is important that the optical alignment which affect the fringe contrast be optimized. The fringe contrast $(I_{max} - I_{min}) / (I_{max} + I_{min})$ is conveniently optimized while observing the fringe pattern created by a monochromatic source such as a Ne or Hg spectral lamps, or laser illumination. A Ne lamp is preferred, because the Hg has a linewidth which is slightly too broad (isotope effect) and creates a visibility 70% of its true value. And the laser makes confusing speckle. For our prototype we observed a Ne lamp visibility of 0.70, allowing a factor of 1.4 times in potential improvement of signal to noise.

The fringe visibility of future EDI could be improved by using better optics. The factors ahead of the spectrograph which affect the fringe contrast include the intensity balance between the interferometer arms, the wavefront error in the beamsplitting surface, the longitudinal superposition of the virtual image of one mirror with the other mirror, and the ability of the relay lens to image vertical detail to the spectrometer slit. Factors after the slit include the ability of the spectrograph to image details in both axes simultaneously. Our HR640 spectrograph had significant astigmatism due to the off-axis reflection of spherical mirrors. This made it difficult to simul-

taneously achieve good fringe visibility and high R. This could be remedied by better optical design.

(The astigmatism was compensated for by offsetting the image plane of lens L5 relative to the slit, since the slit locates the image location in the dispersion direction but not in the transverse direction. Note that if the number of fringes across the beam is reduced, this relaxes the transverse imaging requirement on the optics and can strengthen the signal [fringe amplitude].)

9.2.3. The interferometer stabilization scheme

The phase stepping technique involves taking multiple exposures, where for each exposure the interferometer delay is held constant and between exposures the delay is incremented ideally 90° in phase (quarter wave). Although our data reduction algorithm should be tolerant of large ($\sim 20^\circ$) deviations of the step size from the ideal 90°, it is still desirable to minimize these.

We should emphasize that in contrast to other interferometer techniques, we do not need the delay to be held constant to 1/20000th wave precision in order to measure velocity to 1 m/s. We only need it to be held constant to a 1/8th wave precision. This is because we employ a reference spectrum which is affected similarly (to lowest order) by any microscopic drift in the delay. However, it is possible that our data reduction algorithm, which is still under development, is imperfect and affected in a subtle but significant way by macroscopic drifts in delay. Hence we employ the stabilization to prevent these macroscopic drifts.

During the laboratory tests the short (15 sec) exposures times allowed the phase control of stepping to be done manually. However, for the observatory tests, changing environmental factors of temperature and air pressure (wind gusts) could cause the delay to wander significantly both on the short term and over the ~ 10 minute exposures. Short time scale variations could diminish the fringe contrast averaged over the exposure. Long time scale variations could cause the delay to advance approximately 40 waves over several hours. Although such changes in delay can be compensated for during data analysis, they may create subtle velocity zero point errors and thus should be prevented.

After laboratory tests and prior to observatory tests we developed a closed loop feedback system to

stabilize and control the interferometer delay. A 632.8 nm HeNe laser beam passing through the same section of cavity was used as the probe. This beam generated a fringe ladder of about 4 waves that was recorded by a TV-CCD camera, whose image was sent to a dedicated computer that actuated the PZT using a close loop feedback algorithm written in LabView software (National Instruments, Inc.). Only the piston motion of the interferometer mirror was actuated. Drifts in the mirror tilt which caused significant fringe visibility decrease over the exposure were sometime present during observatory operations. These tilting drifts should be stabilized in a future version of our prototype.

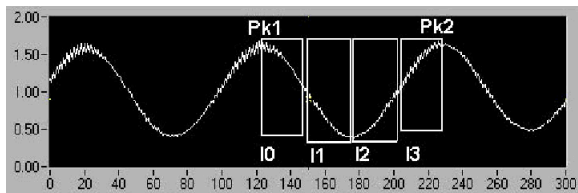


Fig. 21.— Intensity lineout of HeNe laser fringes used for stabilizing the interferometer cavity.

Fig. 21 shows an unfiltered intensity profile across the fringe ladder and the phase step sampling windows used to create four quadrature signals. To establish the quadrants, the algorithm first finds two peaks (Pk1, Pk2) in the ladder and defines the wavelength to span these points.

The intensities are summed within each quadrant to form inputs I_0 , I_1 , I_2 , and I_3 representing the 90° phase steps. The phase stepping algorithm described by Schwider et al. (1993) is used extract the phase ϕ :

$$\tan(\phi + \frac{\pi}{4}) = \frac{2(I_1 - I_2)}{(I_3 - I_2) + (I_0 - I_1)}. \quad (6)$$

This system demonstrated phase locking to a precision of up to $\lambda/400$ in the LLNL lab environment. On the mountain the locking was generally stable to $\lambda/50$, except for those occasional severe wind gusts which were more rapid than the ~ 1 second response time of the electronics. This red HeNe phase measurement was scaled by the ratio of green to red wavelengths and used to command the 90° increment in interferometer delay (for the green starlight) between exposures.

We found that the thermal expansion of the interferometer platform holding the mirrors occasion-

ally exceeded the 25 wave travel range of our PZT transducer trying to stabilize the cavity length, and so periodically we manually translated the mirror to compensate. Future purchase of a longer range actuator will solve this problem. The absolute delay change could be determined from the iodine fringing spectrum by noting the ‘twist’ in the spectrum (phase shift of red end relative to the blue end).

10. Data Taking Procedure

Let the data taken of starlight alone be designated by ‘*Star*’, iodine alone by ‘*Io*’, and starlight through the iodine cell ‘*StarIo*’. Each velocity datum is derived from a *StarIo* dataset, where the dataset optimally consists of essentially 4 exposures taken at 90° phase step intervals. (Three exposures at 120° etc. would also work). Let us call this dataset a ‘quadset’. It is our standard mode of taking all data, *Star*, *Io* and *StarIo*.

The phase stepping allows removal of common-mode noise. This could be due to CCD pixel to pixel gain variations or parasitic fringes from other optical surfaces unrelated to the interferometer, such as the CCD windows. The true fringes can be distinguished by their synchronous variation with the phase stepping. Although flatfield procedures can remove some of this noise, the flat fields are obtained at a different time and thus at a slightly different apparatus configuration than the actual data. Hence, although a single exposure can substitute for the quadset to yield a velocity datum, optimal velocity precision is attained by coherently combining exposures within a dataset.

For each target being observed, even over several sessions, one of the *StarIo* datasets is designated the master *StarIo* to establish a velocity zero. All other *StarIo* will then be compared to this to yield velocity differences. Each target session also requires a *Star* dataset and *Io* dataset as templates. As much as possible, the apparatus configuration is kept the same throughout the sessions, except for the insertion/removal of the iodine cell and the substitution of a white incandescent lamp for the starlight for the *Io* dataset.

At the beginning of a session a Ne or Hg spectral lamp is used for input. Then the instrument is adjusted for maximum fringe contrast, and the interferometer mirror tilt adjusted to set the desired spacing of fringes across the beam. Measuring an *Io*

exposure will indicate the value of the interferometer delay relative to a previous observing session, and the cavity length can then be adjusted to achieve this prior value. Then the cavity stabilization circuit is locked to hold the delay.

An extended series of *StarIo* exposures is made to measure the time dependent velocity of the target. The iodine cell is translated out of the beam to take a few *Star* exposures. Then the iodine cell is re-inserted and the starlight replaced by a white lamp to take a few *Io* exposures. Occasionally, the iodine cell can be translated out of the beam at this point to take a few exposures of a white light fringe comb. (This will require a spectral resolution of $\sim 0.27 \text{ \AA}$ to see the spectral comb.) This provides a count of the number of spectral comb fringes that span the bandwidth of the spectrograph. From this and the Ne lamp lines which establish the exact bandwidth we can calculate the precise interferometer delay and velocity per fringe proportionality. For our 11 mm delay at 5446 \AA average wavelength this was $\approx 14500 \text{ m/s}$ per fringe.

In each configuration, *StarIo*, *Star*, *Io* and *Lamp-only*, several nonfringing exposures are also taken. These are used later to divide out the beam profile from the data, or to assist in flatfielding. Nonfringing spectra are taken by inserting an opaque card into one interferometer arm, then into the other arm, then summing the two exposures.

11. Data Reduction

This hybrid, dispersed-interferometric approach for measuring broadband Doppler shifts is novel to both the dispersive-only and interferometer-only instrument communities, and we needed to develop new mathematical tools for reducing the data. The distinguishing feature is the vector character of the data. Whereas conventional spectra are scalars versus wavelength, the fundamental data format of this instrument is a vector spectrum, which we call a ‘whirl’. The length and angle of each vector represents the fringe amplitude and phase for a given wavelength channel. Under a Doppler shift the entire spectrum shifts in phase, which manifests a rotation (and twist) of the whirl.

The advantage of the vector format is the ability to use many familiar and computationally rapid vector operations such as rotation, addition and subtraction, magnitude multiplication, and the formation of dot products. Since only two degrees of freedom are be-

ing used (fringe phase and amplitude), many sources of noise are excluded when they do not produce the narrowly defined effect of whirl rotation when integrated over the 2500 wavelength channels.

Often systematic error is the limiting factor in instrument performance. Using a multitude of parallel but uncorrelated fringing channels samples systematic error randomly. This reduces the net systematic error to less than that of a single channel by a factor of square root of the number of statistically independent spectral features. This explains how we can measure the phase shift of the iodine spectrum to $\lambda/20000$, (0.76 m/s), which is an order of magnitude better than the state of the art for monochromatic interferogram analysis. Monochromatic interferograms suffer from sampling their systematic error only once.

The whirl is conveniently expressed as a complex signal, where the real and imaginary parts correspond to the rectangular coordinates of the vector. This streamlines many math operations. For example, a complex Fourier transform operation (used during a lowpass filtering) is standard in any data analysis software package and process both real and imaginary parts simultaneously.

The data reduction procedure includes:

1. Removal of cosmic ray events, flatfielding, and dividing out the beam profile.
2. Conversion of each spectrum (2-d intensity image) to a whirl (vector vs wavelength channel), which is represented by a complex signal.
 - (a) The average fringe period along the slit direction is estimated by inspecting the image data.
 - (b) For each wavelength channel, the intensity versus position along the slit direction is Fourier decomposed for the fixed period found above. The sine and cosine Fourier amplitudes are assigned to be the real and imaginary parts of the complex value for that wavelength channel.
3. Coherently combining the (usually 4) whirls of a dataset to form an averaged whirl. The whirls of the dataset are rotated by the estimated phase step existing during its exposure so that they all point in the same direction. Vector addition then creates an averaged whirl. This process discriminates against common-mode errors.

4. Lowpass filtering to extract the moire information.

The whirl is low pass filtered in the wavelength direction to remove any spectral comb created by the interferometer, which occurs at a well defined periodicity. What remains are the moire fringes which contain the Doppler effect. If the spectrograph slit is sufficiently wide, optical blurring will already have accomplished this step.

5. Alignment of every whirl to the same master *StarIo* whirl.

The effects of drifts are removed by rotating, linearly twisting, translating in all three axes, and magnifying each whirl so that it best matches the designated master *StarIo*. Drifts addressed by this alignment include thermally induced change in location of the CCD in the wavelength and fringing axes, brightness changes, and changes in the interferometer delay.

6. Dot product decomposition of each *StarIo* whirl to yield the angle between iodine and stellar component whirls, which becomes the Doppler velocity change.

- (a) The *Star* and *Io* whirl templates are rotated by 90° to form the perpendicular templates $Star_\perp$ and Io_\perp .
- (b) The input *StarIo* is expressed as a linear combination of 4 components consisting of the two template whirls and their perpendiculars. Four coefficients A_\parallel , A_\perp , B_\parallel , and B_\perp to hold the magnitude of each component, with A associated with the *Io* and B with *Star*.
- (c) The generalized dot product is taken between the above expression and each of the four template whirls. This creates four equations in the four unknown coefficients, using the fact that the dot product between the templates yields either zero or a constant. The generalized dot product between two whirls is defined to be the sum over all wavelength channels of the channel by channel dot product.
- (d) The four linear equations are solved by matrix algebra to yield the four coefficients.

- (e) The arctangent between A_\parallel and A_\perp yields the angle of the iodine component whirl, and between B_\parallel and B_\perp the angle of the stellar component. The difference between the two is the angular separation.
- (f) The angular separation is multiplied by the velocity per fringe coefficient (14500 m/s) to yield the change in Doppler velocity between the master and input *StarIo* datasets.

The vector operations are computationally very fast due to their massively parallel nature. Presently the algorithms are written in high level script of a commercial data analysis environment (Igor Pro, Wavemetrics Inc., Lake Oswego, OR). Even in this un-optimized state the code executes on a Macintosh G3 computer at about 2 minutes per datum. Porting key kernals of the algorithms to a direct language such as C or Pascal would boost performance even further.

12. Measured performance of the dispersed interferometer

In order to measure the technique's performance, we conducted experiments with two versions of the prototype in two locations. The earliest prototype was tested in the lab, and a later version with cylindrical optics, cavity stabilization, and a fiber-feeding interface was tested at Lick Observatory 1m telescope. The performance shows very promising results at both sites, but also shows which technical problems need to be addressed in future experiments.

12.1. Lab performance

The earliest prototype was tested in the lab for the purpose of exploring and validating the velocimetry aspect of the instrument concept, rather than its efficiency potential. For expediency, means for converting the round input beam shape to a narrow rectangle was not employed. Consequently most photons were lost at the slit, and we were limited to bright sources. Using sunlight we were able to detect the diurnal acceleration of the Earth and saw fluctuations similar in character to the known 5-minute oscillations of the photosphere. However, we could not rule out the possibility that our roof mounted heliostat used for tracking the sunlight may have flexed with the wind and introduced additional velocity noise due

to the steep ~ 4000 m/s rotational gradient across the solar disk. Consequently we abandoned sunlight as a velocity calibrant until a future time when the heliostat can be improved.

This points out the challenge in determining instrument performance on a 1 m/s scale: we found no convenient and bright natural source that is sufficiently velocity-quiet. The natural solar oscillations of the sun would obscure our instrument noise.

Hence we adopted the bromine absorption cell backlit by white light as a convenient and bright constant (zero) velocity source. Like the iodine spectrum, the bromine spectrum has many features in the green region of interest and these are sufficiently different than the iodine spectrum. (The dot product between bromine and iodine whirls is sufficiently smaller than either self-dot product.)

However, we have not yet verified the long term constancy of the bromine cell in the configuration we used. In the tests the bromine temperature (and hence column density) was not regulated, and the optical density was unusually high. Changes in the optical depth could have created changes in the perceived velocity because the small signal approximation was not perfectly valid. That is, at high optical density the true effect of transmission through the Br and I₂ cells in series is a multiplication, rather than the assumed addition of the bromine and iodine absorption spectra. When the bromine is optical dense, which it was, this generates new nonlinear mixing terms that vary with optical density, and hence temperature & pressure of the cell, which was unregulated. For expediency these were ignored in our data reduction. However, it would be straightforward to modify the algorithms for account for this. Another simple future remedy is to regulate the bromine cell temperature and to use a weaker optical depth.

We conducted a series measurements using the bromine spectrum as a simulated source substituting for star light. White light from an incandescent lamp passed through both a bromine and iodine vapor cell. The grating operated in the 2nd diffraction order. The slit was sufficiently narrow to partially resolve the continuum interferometer spectral comb, which had fringe visibility of 13%. In comparison the Ne lamp produced a 70% visibility, in 5 fringes along ~ 60 pixels in the slit direction and a 5.5 pixel (0.27 Å) FWHM peak in the dispersion direction. Hence R was approximately 20000 at 5400 Å. The bandwidth across the 2500 CCD channels was 124 Å.

Exposures were made every 15 seconds while phase stepping, over a period of about 18 minutes and grouped into quadsets to produce 17 velocity data. The fifth datum was assigned to be the master *StarIo* and hence defined zero velocity. All other data, including sessions taken several days later, referred to this master *StarIo*.

Fig. 12 shows the measurement results. During the first 18 minutes the apparent velocity was measured with a repeatability of 0.76 m/s. This value includes both instrument and photon noise, but we believe from Monte Carlo calculations that the value was dominated by photon noise. Hence the short term instrument noise could be much less than 0.76 m/s. (Based on the number of counts collected and 2.8 electrons per count, the number of photoelectrons was estimated to be 5.2×10^9 per datum for the first session, shown at left of Fig. 12).

What is remarkable about the result is that it shows it is possible to break the 1 m/s precision milestone with an inexpensive instrument, using a small grating with a PSF approximately 3.5 times coarser than that used in conventional Doppler spectrometers, (which have $R \geq 20$ k). This is accomplished through the effect of heterodyning, which can be thought of as multiplying the input spectrum with a very regular sinusoid *before* the blurring of the spectrograph occurs.

A practical instrument for the Doppler planet search must also have velocity stability over the long term. The second and third data sessions of Fig. 12 were taken after 3 hours, and again after 11 days, using the same *Star* and *Io* templates and master *StarIo* of the first session. (The fluxes were slightly less, 4.6 and 3.5×10^9 photoelectrons per datum for the middle and right sessions, respectively). The results show long term drifts of not more than 4 m/s, and the drift after 11 days was ~ 1 m/s. We have not yet ruled out that the unregulated temperature of the bromine may be the source of this drift. However, this value is already competitive with the ~ 2 m/s instrument error of the best conventional spectrometers, many of which are mature designs and located in protected environments. Our instrument was constructed of lenses-on-posts breadboarded in the open air. We fully expect that stabilizing the environment around our instrument will greatly reduce our long term drifts.

12.2. Performance at the Lick 1m

In December 1999, we coupled our fiber-fed EDI to the Lick 1m telescope over a 10 night engineering run for initial starlight testing. The instrument, consisting of optics on posts mounted in open air on a breadboard, was set up in the telescope dome without environment protection or control. The most significant optical difference in the instrument from the lab configuration was the 3.5x coarser resolution of the spectrograph. This was due to the use of the grating in 1st order instead of 2nd order (to boost flux), and a somewhat wider slit. The bandwidth across the 2500 pixels was 343 Å. A Hg lamp produced a peak on the CCD with 7 pixel FWHM (0.96 Å) corresponding to $R = 5600$ at 5400 Å (in comparison to $R=20000$ in the lab configuration). This resolution was too coarse to detect the continuum spectral comb fringes (having periodicity of 0.26 Å), which were partially resolved in the lab configuration.

Fig. 17a shows 800 pixels (out of 2500) of the raw fringing spectrum observed from a nearby bright star, Arcturus ($V = -0.04$ mag, K1.5III variable). Faint vertical moire fringes can be seen, with about 3–4 fringe periods across the spectrum width. The hump-like transverse profile of the spectrum may make the few percent contrast fringes difficult to discern in the photograph. The fringe visibility was consistent with that of the solar spectrum taken with the same instrument configuration during the day.

Fig. 17b shows the fringes of Fig. 17a after data reduction, essentially after the image has been flattened and all nonfringing components in the transverse direction removed. This shows the coherently averaged whirl obtained after data reduction step 3. In this pseudofringe method of displaying vector spectra, the vector magnitude and angle for each wavelength channel is represented by a synthetic fringe in a 2-d intensity map having corresponding amplitude and phase, and fixed periodicity of 32 pixels unrelated to the actual periodicity. The black and white limits of the grayscale range of Fig. 17b correspond to $\pm 9\%$. The whirl depicted here was used as the *Star* template.

Figures 17b and 17c show *Io* and *StarIo* whirls with grayscale limits corresponding to $\pm 10\%$ and $\pm 11\%$, respectively. Note that *StarIo* appears consistent with being a vector sum of *Star* and *Io*, as presumed in the data analysis. Note also that the *Io* whirl contains more fringing energy than the *Star* whirl, as indicated by the generalized self-dotproduct

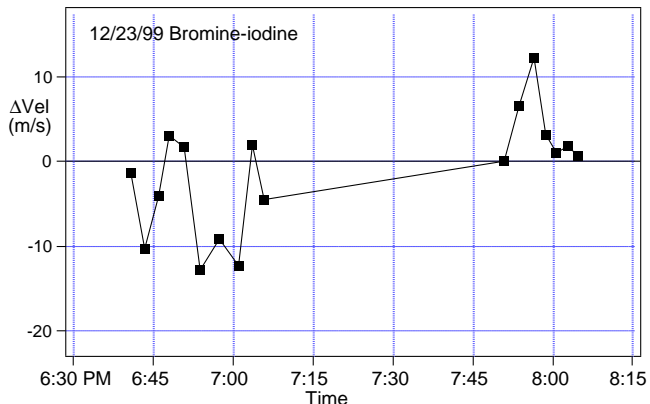


Fig. 22.— Zero velocity repeatability by the fiber-fed EDI at the Lick 1m telescope during the December run in 1999. Bromine absorption cell is used to simulate a zero velocity Doppler source for the measurement. This differs from the analogous measurement made in the lab by the 3.5x coarser spectrograph resolution (5600 vs 20000).

$|Star|^2$ being 3.5x greater than $|Io|^2$. For green wavelengths the *Io* whirl contains more fringing energy per bandwidth than *Star*, for bandwidths up to about 800–1000 Å. Redder than ~ 6000 Å, iodine does not contribute new significant fringing lines while the stellar spectrum does. Hence from a signal to noise standpoint, in future schemes it would be worthwhile to increase the *Star* bandwidth to be at least 3.5x as wide as the iodine range (to ~ 3000 Å), until the two whirl self-dotproducts equalize, before the benefit per additional bandwidth diminishes.

Figure 14 plots the change in Doppler velocity versus time measured for Arcturus over a 55 minute session. The first datum was arbitrarily assigned zero velocity and the diurnal acceleration of the Earth has been removed from the data. Due to the reportedly unstable nature of this star’s photosphere, its lack of planets, and the relatively short duration of the session, the Arcturus velocity data by itself is of little use except as a first-light exercise in using the entire instrument system under observatory conditions. We intend to install flux enhancing improvements to the apparatus which will allow us to observe a wider choice of stars, particularly those having less intrinsic velocity noise.

In order to measure the Doppler precision of the prototype at Lick, we conducted repeatability tests using the bromine absorption cell source with the instrument in the same configuration used to observe Arcturus. Fig. 22 shows the apparent velocity of

bromine spectrum relative to iodine, taken in two sessions over about 70 minutes. The datum at about 7:51 pm defines zero velocity. The repeatability is about ~ 7 m/s.

This precision is 7–10 times worse than that obtained in the lab. We believe this is mainly due to the wider slit which blurred the moire fringes and prevented resolution of the continuum spectral comb. The former effect reduced the signal and the latter increased the susceptibility of the algorithms to noise. In addition, we have not yet determined the role temperature variation of the bromine may have contributed. In principle a different spectrograph having $R = 20$ k could be used for starlight operations, and we expect that we would recover the ~ 1 m/s scale instrument noise we observed in lab tests.

12.3. Signal to noise ratio versus slit width

The average fringe magnitude observed in the Lick configuration was measured to be 2.5x smaller than that observed in the lab configuration. This contributes a factor 2.5x reduction in the SNR. This decrease was due to the blurring of fringes due to the coarser spectral resolution ($R=5.6$ k vs $R=20$ k) of the spectrograph used at Lick than in lab tests.

Secondly, the susceptibility of the data reduction algorithm to noise insult doubled between the lab and Lick configurations. This was determined through a numerical simulation, where random noise was added to the fringing spectra and the amount of increased velocity noise was noted. This contributes a factor 2x to the SNR. The origin of this increased susceptibility is the lack of spectral comb in the Lick configuration due to increased blurring. Recall that the spectral comb are the sinusoidal fringes created by action of the interferometer on the continuum portion of the input spectrum. (The moire fringes are the fringes created by action of the interferometer on the absorption lineshapes.) Even though the spectral comb does not carry any Doppler information, it acts as a dummy signal that provides significant fringing energy in every wavelength channel. This provides a more accurate location of the rotational center of the whirl, which reduces error during rotational and twisting manipulations. This contributed a factor 2x increase to the signal to noise ratio.

Furthermore, the input noise itself was measured to be approximately a factor 1.4x larger at Lick, possibly due to the drifting phase, between exposures, of

parasitic fringes observed in the data. These parasitic fringes are due to optical surfaces other than the interferometer. Because of their systematic pattern they can be identified and removed from the data in the future.

Thus we can account for an increase of a factor $(2.5)(2)(1.4) = 7$ in the SNR between lab and Lick configurations, which is consistent with the observed increase. This is a configuration dependent change that should be reversible. After installing a procedural step to deduct the parasitic fringes, returning the instrument spectrograph to 0.27 Å or less slit width should reproduce a ~ 1 m/s precision capability.

13. Transmission efficiency at Lick

The starlight testing at the Lick 1m demonstrates that the EDI can be used for sensitive Doppler radial velocity measurements of nearby bright stars. However, the instrument efficiency at the Lick 1m was much below its potential (ie., being $\sim 2\%$ instead of $\sim 30\%$). Although this is not terribly lower than the 5–15% typical of conventional Doppler spectrometers. Our low transmission prevented us from observing stars fainter than $V = 3$ mag. in a half hour integration. Strategically, we chose to develop and explore the velocimetry capability first, since this was the least understood. Now efficiency is a critical issue. We intend to address and improve each portion of the instrument design which effects detected flux. Some ideas have been discussed in sections 9.2.1 and 9.2.2. These include construction of a custom-designed high efficiency spectrograph, an interferometer that uses both outputs, better beamshape conversion, and better fiber-feeding design.

14. Discussion

Dispersive interferometry is a new approach for precision Doppler radial velocity, and has potential beneficial spin-off applications for general purpose spectroscopy. Numerous advantages include a much simpler instrument response function using only 2 degrees of freedom. This lowers instrument noise, and the vector based mathematics speed computation. A heterodyning effect allows the use of compact, 3–4x coarser resolution spectrographs than conventional technology to achieve ~ 1 m/s precision radial velocimetry. Grating PSF variations no longer directly manifest velocity errors, because the velocity is determined in the transverse direction to the disper-

sion axis. Hence, tolerances on many design aspects are greatly relaxed.

For example, this allows the use of both emission lamps or absorption cells for spectral reference. This in turn permits the interferometer be more easily used in wavelengths (such as the important infrared region) other than the current green iodine absorption wavelengths for Doppler planet searches. This will boost flux from M stars, allowing them to be included in Doppler surveys where they are currently under-represented. The relaxed design tolerances allow engineering choices which can increase efficiency closer to its theoretical maximum. Grating technologies (such as volume holographic gratings) which have high diffraction efficiency can be employed with less regard to their PSF, since the role of detecting velocity has shifted from the grating to the interferometer. Because all wavelengths travel the same (split) path through the interferometer, its frequency response is more mathematically regular than a grating.

The consequence is that slits can be opened up, and larger diameter fibers for conducting starlight can be used. This makes it less expensive to couple the spectrometer to large area light collectors, which can provide large numbers of photons. When these large fluxes are present, the lower instrument noise allows new time-resolved studies of stellar oscillations which will provide important information on stellar interior structure.

Acknowledgements

Thanks to Dr. Charles Alcock for useful discussion and assistance, and to Dr. Gibor Basri for lending us a bromine cell. We are grateful to the personnel of Lick Observatory (University of California) for their hospitality and use of the Nickel 1m telescope. Thanks to Neil Holmes, Ed Moses and Dick Treffers for unflagging support and encouragement. We relied on Ken Visbeck for precision crafting of hardware and careful transportation of equipment to and from Lick. This work was supported by Laboratory Directed Research and Development funds. This work was performed under the auspices of the U.S. Department of Energy by University of California Lawrence Livermore National Laboratory under Contract W-7405-Eng-48.

REFERENCES

- Allen, C.W. 1973, *Astrophysical Quantities*, The Athlone Press, London.
- Baranne, A., Queloz, D., Mayor, M. et al. 1996, *Astr. & AstrPhys Suppl.* 119, 373-390
- Beer, R. 1992, *Remote Sensing by Fourier Transform Spectroscopy*, Wiley & Sons, p66.
- Butler, R. P., Marcy, G.W., Williams, E., McCarthy, C. Dosanjh, P., & Vogt, S. 1996, *PASP*, 108, 500
- Dohi, T. Suzuki, T. 1975, *Appl. Opt.* 5, 1137-1140
- Douglas, N. 1997, *Proc. Ast. Soc. Pacif.* 109, 151-165
- Marcy, G.W., & Butler, R.P. 1998, *ARA&A*, 36, 57
- Erskine, D.J., & Ge, J. 1999, in *Imaging the Universe in Three Dimensions: Astrophysics with Advanced Multi-Wavelength Imaging Devices*, (ASP series) 195, 501
- Henry, T. 1991, Ph.D. Dissertation, The University of Arizona
- Hilliard, R. L., & Shepherd, G. G. 1966, *J. Opt. Soc. Am.*, 56, 362
- Kirkpatrick, D.J., Kelly, D.M., Rieke, G.H., Liebert, J., Allard, F., Wehrse, R. 1993, *ApJ*, 402, 643 Ref 11
- Santos, N., Mayor, M., et al. 2000, *Astr. & AstrPhys.* July 20
- Schwider, J., et al. 1993, *Optical Engineering*, 32(8), 1883